2009-01-01

Assessing Repeatability Of Four-Point Bending Method For Estimating Fatigue Cracking Of Hot Mix Asphalt

Sara -. Montazeri
University of Texas at El Paso, smontazeri@miners.utep.edu

ASSESSING REPEATABILITY OF FOUR-POINT BENDING METHOD FOR ESTIMATING FATIGUE CRACKING OF HOT MIX ASPHALT

SARA MONTAZERI

Department of Civil Engineering

APPROVED:

Soheil Nazarian, Ph.D., Chair

Vivek Tandon, Ph.D.

Jack Chessa, Ph.D.

Patricia D. Witherspoon, Ph.D.
Dean of the Graduate School

ASSESSING REPEATABILITY OF FOUR-POINT BENDING METHOD FOR ESTIMATING FATIGUE CRACKING OF HOT MIX ASPHALT

by

Sara Montazeri, BSCE

THESIS

Presented to the Faculty of the Graduate School of

The University of Texas at El Paso

in Partial Fulfillment

of the Requirements

for the Degree of

MASTER OF SCIENCE

Department of Civil Engineering

THE UNIVERSITY OF TEXAS AT EL PASO

December 2009

Acknowledgements

I would like to express my gratitude to Dr. Soheil Nazarian, Professor of Civil Engineering at the University of Texas at El Paso, for his guidance and ever-present support and during all stages of this study. His continuous encouragement, insight, and direction brought this study to its completion. The privilege of working with him has been a rewarding experience; both academically and professionally.

Especial acknowledgment to Mr. Jose Garibay, the Laboratory Coordinator at the Center for Transportation Infrastructure Systems, for his ever-present and unconditional support during all stages of this study. ¡Gracias Jose!

Thanks to Mr. Imad Abdallah, Associate Director in the Center for Transportation Infrastructure Systems for his assistance pursuing this research.

I appreciate the help I received from Mr. Manuel Celaya, Mr. Sergio Rocha, and the entire faculty and staff of the Department of Civil Engineering and the Center for Transportation Infrastructure Systems.

I am very thankful to my co-workers; Mr. Jose Moran, Mr. Hector Hernandez, for their assistance during laboratory works which brought this study to completion.

I note with heartfelt gratefulness the unconditional support of my family. Most especially my husband, Mr. Milad Zarei and my parents, Mr. Ali Akbar Montazeri, and Mrs. Simin Heidari, who supported, tolerated, and encouraged me throughout the course of this study. Merci!

Abstract

The objective of this thesis was to assess the repeatability of four-point bending method for estimating fatigue cracking of hot mix asphalt. This experimental research examined the influence of mix proportions, specifically asphalt and air void contents, on fatigue behavior of asphalt beam specimens in the laboratory tested with four-point bending method of loading. Following the relevant specifications, the strain-controlled mode of loading was selected. Fatigue failure is expected to occur at the cycle which the flexural stiffness of asphalt specimen reduced to 50% of initial amount. Up to a 1,000,000 cycles of loading were applied to each specimen.

Different tests at different temperatures and loading frequencies were conducted on a synthetic specimen and four different asphalt mixes. The applied strain varied between 200 and 600 με, temperature varied between 4.4 and 37.5 ^{o}C) and loading frequencies of 5, 10, and 15 Hz were used.

Based on repeated tests on a synthetic specimen, the device evaluated here was very repeatable. However, tests performed on hot mix asphalt specimens yielded a variability of up to 30% which can be mostly attributed to the variability of the specimens.

Temperature impacted the fatigue properties of a given mix the most. A decrease in temperature results in an increase in mix stiffness and consequently a decrease in laboratory fatigue life of specimens. The least fatigue resistance was obtained for specimens tested at 4.4^{o}C. A number of specimens at that temperature failed before the full number of cycles could be applied. The differences in the fatigue properties of specimens tested at 21.5 and 37.5 ^{o}C were more similar than those tested at 4.4 ^{o}C.

The impact of the frequency on the measured parameters in the range of frequencies of 5 to 15 Hz is rather small and within the magnitude of uncertainties anticipated due to variations in the uniformity of the specimens. Typically tests performed at a load frequency of 15 Hz resulted in lower fatigue parameters than those at 5 and 10 Hz.

The nominal air void contents are directly related to the fatigue parameters. An increase in air-void content resulted in a decrease in the laboratory fatigue life and a decrease in mix stiffness.

Another important consideration in this test method is the quality of the specimens. With respect to fatigue performance, accurate control of air-void content is very important. A cyclic loading method was used to prepare the specimens in this study. It was found that the control of the density of the specimens after trimming was difficult. Several specimens with very close bulk densities after compaction yielded variable overall air voids after trimming. An ultrasonic device is recommended as a tool for quality control before fatigue testing of the specimens.

Table of Contents

List of Tables

List of Figures

CHAPTER 1

Introduction

Hot mix asphalt (HMA) is defined as a mixture of well graded aggregates combined with an asphalt cement binder to provide a stable structure for passing vehicles. As the upper layers of road pavement, hot mix asphalt (HMA) mixtures are designed to resist aging and distress that are induced by load repetition and environmental conditions, especially temperature. To provide a smooth and stable surface, HMA should be compacted to a required density based on the existing standards and guidelines.

HMA distresses can be divided into two main modes: fatigue cracking and rutting. These failure modes significantly reduce the asphalt pavement serviceability. To enhance asphalt pavement performance, it is necessary to improve the characteristics and structural resistance of HMA to those failure criteria. To obtain the optimum design thickness for pavement layers with a desired life, improving the asphalt binder, aggregate properties, and improving construction quality are beneficial.

The most common tests to predict the fatigue resistance life are the bending beam and indirect tensile fatigue tests. The main objective of this thesis is to assess the performance of a popular bending beam fatigue test device manufactured by IPC, Inc. The fatigue beam device is useful for predicting the fatigue life of asphalt specimens by measuring the modulus and flexural stiffness and other parameters such as phase angles, and tensile strain for each load cycle and frequency. To achieve this objective, results based on variable air void contents using the four-point fatigue beam test machine were studied.

1.1 OBJECTIVE

The following list contains the main objectives of this research:

- Study the repeatability of data due to the performance of the IPC machine as a four-point bending device for asphalt fatigue testing
- Study the effect of temperature as an environmental factor, and also the mix properties such as air voids content on fatigue life of HMA
- Study the impacts of frequency of loading and strain variation on fatigue performance of asphalt beam specimens

1.2 ORGANIZATION OF REPORT

This thesis has been divided into five chapters. Chapter 1 includes the introduction of objectives, and scope of work. Chapter 2 contains a review of relevant literature regarding asphalt fatigue life which is followed by a summary of other researches adopted by several organizations and state agencies. Some of the conventional and recently developed asphalt fatigue test methods are mainly reviewed. Chapter 3 presents mechanisms, causes and factors of fatigue cracking for experimental set up and design and test procedure. Chapter 4 contains the test results for the fatigue beam tests. Chapter 5 presents the conclusions and recommendations of this study. All supporting test data and additional graphical plots are included in the appendices.

CHAPTER 2

Background

Mechanistic-empirical (ME) design methods have become more popular in the last decade. The major input parameters to these design programs are the traffic loading (volume and type), soil-support (including drainage considerations), and mechanical properties of different pavement layers and their changes with environmental factors.

For the hot mix asphalt (HMA) layer, the distresses listed in Table 2.1 negatively impact the performance of flexible pavements. These distresses can be structural or functional, and may or may not be load associated. The main two structural, load-associated distresses are the fatigue cracking and rutting.

HMA layer fatigue cracking can be considered as one of the primary asphalt pavement distress that reduces the performance of the asphalt layer (Paris et al., 2002). The mechanism of fatigue cracking through the pavement layers is shown in Figure 2.1. It has been common to assume that fatigue cracking normally initiates at the bottom of the asphalt layer and propagates to the surface (bottom-up cracking). With the repetition of wheel loads on the pavement, the highest tensile strain initially occurs at the bottom of the HMA layer. In simple terms, the fatigue cracking is related to the modulus ratio of HMA and the adjacent layers. Environmental factors, such as temperature changes, directly impact this modulus ratio because of viscoelastic characteristics of asphalt mixtures.

Table 2.1 – Possible Types of Distress that Create Failures in Asphalt Pavement

Type of Distress	Structural	Functional	Load	Non-Load
Alligator or Fatigue Cracking	*		*	
Rutting	*		*	
Longitudinal and Transverse	*			*
Block Cracking	*			*
Corrugation		*		*
Depression		*		*
Lane/Shoulder Drop off or Heave		*		*
Lane/Shoulder Separation		*		*
Bleeding		*		*
Polished Aggregate		*	*	
Raveling and Weathering		*		*

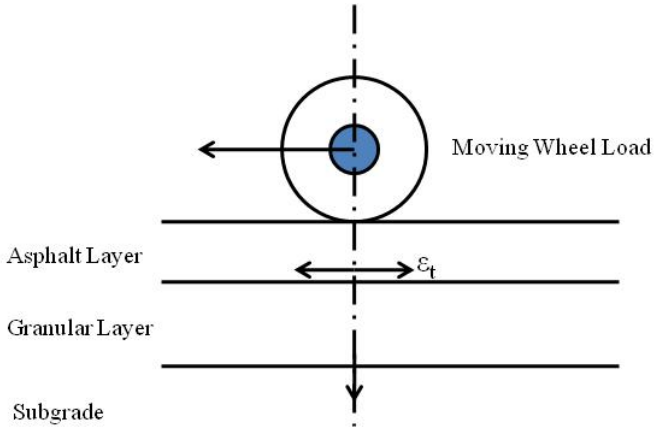

Figure 2.1 – Fatigue Cracking Principle (Brown, 1996)

The amount of fatigue cracking is also influenced by the thickness of the HMA layer (Kaloush et al., 2002). The crack width has a relation to loading cycles which can be modeled

with an exponential function. The shapes of cracks are almost semielliptical and the length and depth of cracks are proportional to each other (Brown et al., 2001).

Recent studies have also demonstrated that fatigue cracking may also be initiated from the top and propagate down (top-down cracking), (Kaloush et al., 2002 and Mun et al., 2006). This type of fatigue is not as well defined from a mechanistic viewpoint as the more classical "bottom up" fatigue. Generally, it is assumed that critical tensile and/or shear stresses develop at the surface and cause extremely large contact pressures at the tire edges-pavement interface, coupled with highly aged (stiff) surface layer that have become oxidized.

Fatigue life is defined as the ability of asphalt to respond under repeated traffic loading and prevailing environmental conditions without causing significant cracking. The most important factor in fatigue criterion is the allowable number of repetitions at a given stress ratio between flexural tensile stress and the tensile strength. Almost every fatigue model developed and presented in the literature follows the form of (Li and Metcalf, 2004):

$$N_f = K_1[1/\varepsilon_{cr}]^{k_2}[1/E_s]^{k_3} \quad (2.1)$$

where N_f = the number of repetitions to fatigue cracking, ε_{cr} = tensile strain at the critical location (typically bottom of the HMA layer) and E_s = modulus of the material. Parameters k_1, k_2 and k_3 are empirical calibration parameters.

To investigate crack initiation and propagation, the fatigue crack should be simulated by conducting laboratory tests on asphalt specimens and evaluating the intensity factor using fracture mechanics models by calculating the stress intensity factor (SIF) from linear elastic fracture mechanics (LEFM). According to Li and Metcalf, (2004), the Paris law was used by Majidzadeh et al. (1971); Carpenter and Lytton (1978); Lytton and Shanmugham (1982) and

Molenaar (1983) to model the crack propagation rate. Equations 2.2 and 2.3 show the formulation of this process (Li and Metcalf, 2004):

$$\frac{d_c}{d_N} = A\,K_c^n \tag{2.2}$$

$$N_f = \int_{co}^{cf} d_c \Big/ A\,K_c^n \tag{2.3}$$

where dc/dN = the rate of crack propagation, K_c^n = stress intensity factor (SIF) corresponding to the crack size of C, A and c= material constants, N_f is fatigue life, c_0 = initial crack length, and c_f= critical crack length.

Thom (2006) studied the development and propagation of cracks under repeated load using different laboratory testing configurations under different temperature and loading rates. Thom proposed a unique relation between the asphalt life serviceability and tensile strain (ε_t).

Raad et al. (2001) performed strain-controlled flexural beam testing at pre-defined frequencies and temperatures to characterize the cracking of HMA mixes. They found that the field aging reduced the beam fatigue resistance potential.

2.1 METHODS FOR ESTIMATIONS FATIGUE CRACKING

Tangella et al. (1990) contains a chronological history of early work done in estimating the fatigue behavior of mixes and corresponding test methods. These test methods follow different principles to stimulate the loading condition for asphalt specimens. In the laboratory, two types of controlled loading are generally applied for fatigue characterization: constant stress and constant strain. In the case of constant strain test, the strain remains constant with the number of repetitions (See Figure 2.2). Because of the damage due to repetitive loading, the applied stress reduces resulting in a reduced stiffness as a function of repetitions.

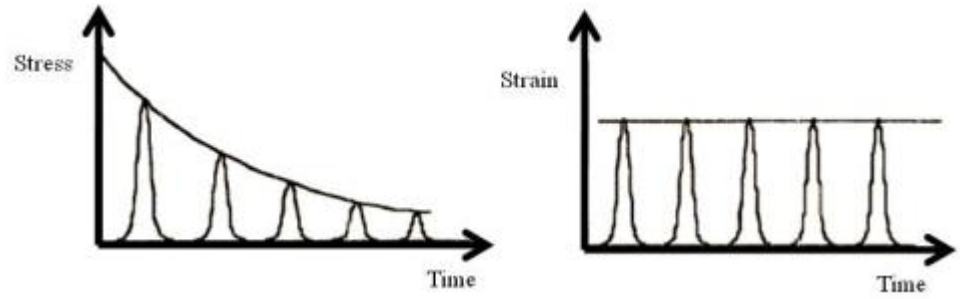

Figure 2.2 – Schematics of Stress and Strain Behavior under Strain-Controlled Condition

In constant stress testing, the applied stress during the fatigue testing remains constant. As the repetitive load causes damage in the test specimen the strain increases, resulting in a lower stiffness with time (see Figure 2.3). The constant stress type of loading is considered applicable to thicker pavement layers usually more than 200 mm (8 in.). Because of the different stress states and damage mechanism for different thicknesses of the asphalt layers, the fatigue model employed in the Mechanistic-Empirical Pavement Design Guide is the constant strain and constant stress models developed by Shell Oil (Kaloush et al., 2008).

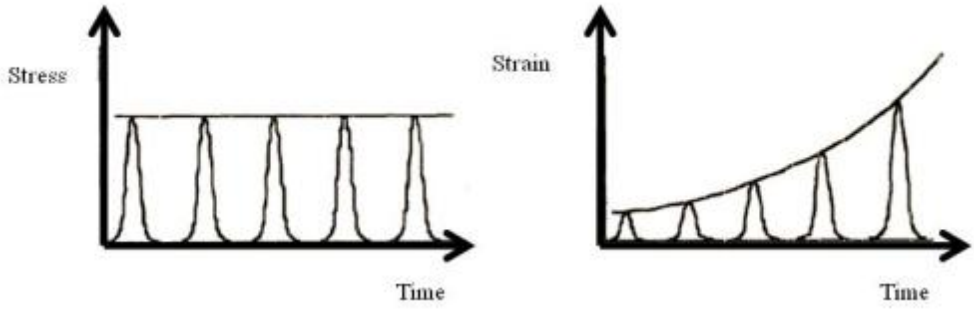

Figure 2.3 – Schematics of Stress and Strain Behavior under Stress-Controlled Condition

2.1.1 Simple Flexure

The majority of fatigue test methods have been developed by simple flexure tests in which the stress or strain is repeatedly applied until the specimen fails or exhibits changes in characteristics which rendered the mixture unsuitable. The common methods are the center-point or third-point loading flexure tests (see Figure 2.4).

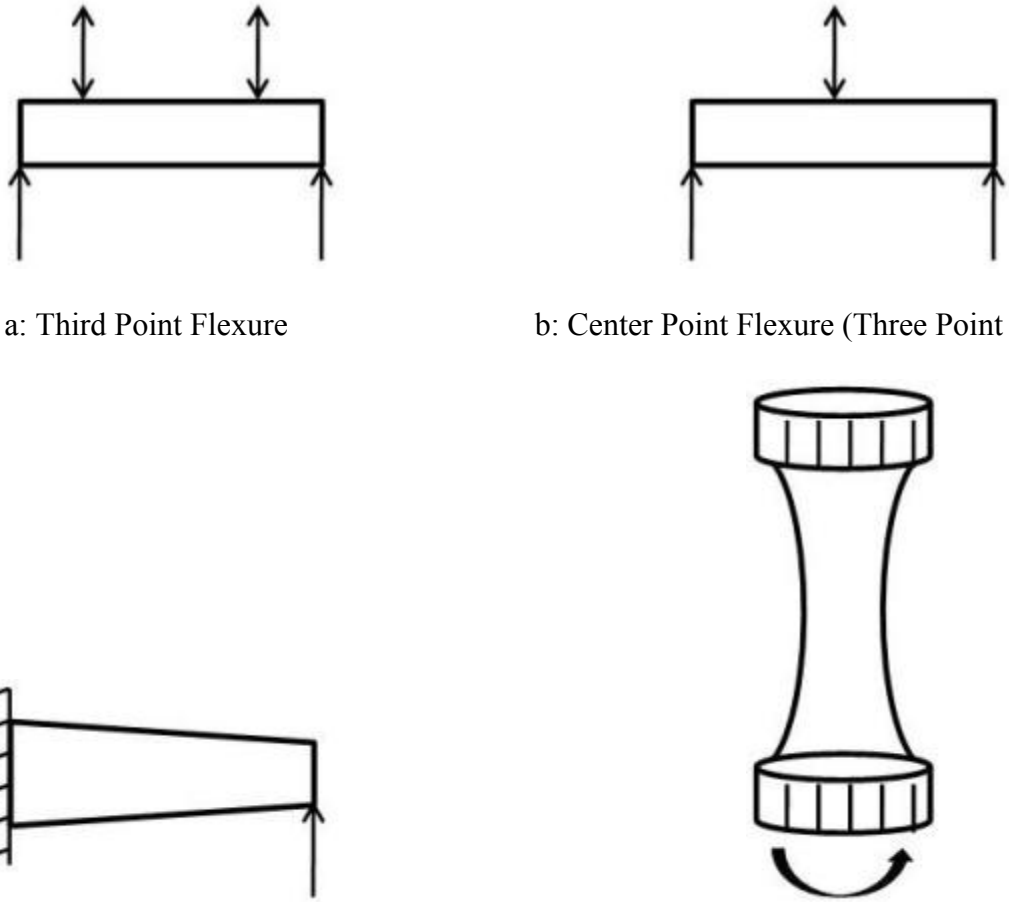

a: Third Point Flexure

b: Center Point Flexure (Three Point Bending)

c: Cantilever(Two point Bending)

d: Rotating Cantilever

Figure 2.4 – Loading Configuration of Different Flexure Tests

In rotating cantilever test method, the specimen is mounted vertically on a rotating cantilever shaft and a load is applied at the top, while the bending stress of constant amplitude is

induced through the specimen. In this method, elastic theory is usually assumed to compute the tensile strain or stress. Although this method is well known to measure the fatigue failure, it is costly, time consuming, and requires specialized equipment.

In the third point bending flexure test, rotating cantilever and axial test, the fatigue failure occurs in a uniform bending moment or tensile stress zone. In flexure test methods, a haversine or sinusoidal loading is used except for the rotating cantilever. In rotating cantilever test, a continuous sinusoidal loading waveform is used which is different from other flexure methods.

2.1.2 Supported Flexure

This method is used directly to simulate in-situ modes of loading and sometimes to simulate a more representative stress state as shown in Figure 2.5. Beams or slabs that are supported in various ways to directly simulate in-situ modes of loading are loaded to simulate a more representative stress state. Because the specimen is supported, the effects of minor imperfections in the specimens are small, improving the repeatability of the test results (Tangella et al., 1990).

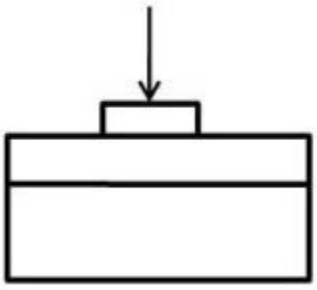

Figure 2.5 – Loading Configuration of Supported Flexure Test Method

2.1.3 Direct Axial

Uniaxial tension and compression tests are performed by applying a haversine strain-controlled loading as shown in Figure 2.6. It is important to mention that, the loading condition does not match always the same as the field condition, so the results in some conditions are not as realistic. Compared to flexure tests, this method is simpler and cheaper.

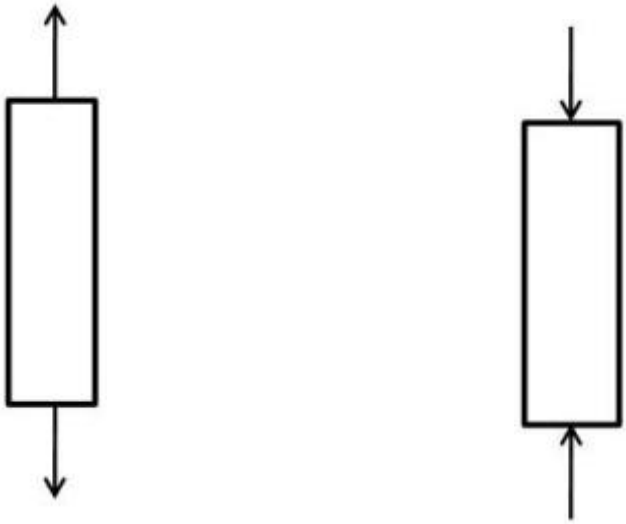

a: Tension Condition b: Compression Condition

Figure 2.6 – Loading Configuration in Direct Axial Test Method

2.1.4 Diameteral Fatigue

The diameteral fatigue test is an indirect tensile test conducted by repetitively loading a cylindrical specimen with a compressive load which acts parallel to and along the vertical diameteral plane. This loading configuration develops a reasonable uniform tensile stress in the specimen perpendicular to the direction of the applied load and along the vertical diameteral plane (sees Figure 2.7). The state of stress is biaxial.

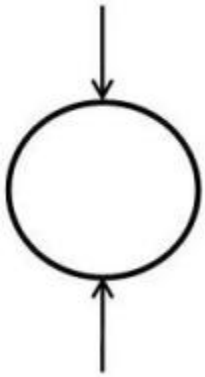

Figure 2.7 – Diameteral Test Method

2.1.5 Triaxial

The triaxial test procedure is similar to direct axial testing but under a confined condition. Based on the test equipment type, the loading is configured. The compression is followed by tension because of the loading condition, so it can stimulate the field loading very well.

2.1.6 Fracture Mechanics Principles

In the fracture mechanics models, the fatigue failure is considered to develop in three phases. First, crack initiation, then the stable crack growth, and as the final phase the crack propagation (Tangella et al., 1990).

Understanding the micromechanics of cracking of pavements relies on knowledge of the fracture of bituminous mixes, which ultimately needs to understand the fundamental fracture properties of pure bitumen. Harvey and Cebon (2005) performed 3-point bend tests on pure bitumen and asphalt mix to characterize the fracture behavior over a wide range of temperature and loading rates. A wide range of crack behavior was observed, from brittle to ductile.

Fracture parameters such as the Mode I fracture toughness, K_{IC},; fracture energy, G_{IC},; crack mouth opening displacement, Δ; and J integral, J_{IC}; were derived from the tests(See Table 2.2 from Portillo, 2008).

Table 2. 2 – Fracture Characterization Parameters and Formulas for the Single Edge Notch Specimen

Parameter	Applies to	Formula	Notes
Stress Intensity Factor, KIC	**Linear Elastic Materials**	$K_{IC} = \frac{PS}{BW^{3/2}} Y(a/W)$ $Y(a/W) = \frac{3\left(\frac{a}{W}\right)^{1/2}\left[1.99 - \frac{a}{W}\left(1-\frac{a}{W}\right)\left(2.15 - 3.93\frac{a}{W} + 2.7\left(\frac{a}{W}\right)^2\right)\right]}{2\left(1+2\frac{a}{W}\right)\left(1-\frac{a}{W}\right)^{3/2}}$	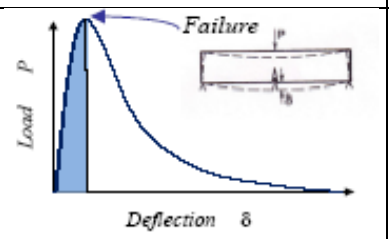
Fracture Energy , GIC	**Linear Elastic Materials**	$G_{IC} = \frac{\int_0^{\delta_{max}} P(\delta)d\delta + \frac{1}{2}Mg\delta_{max} + \int_0^{\Delta_{max}} F_s d\Delta}{B(W-a)}$	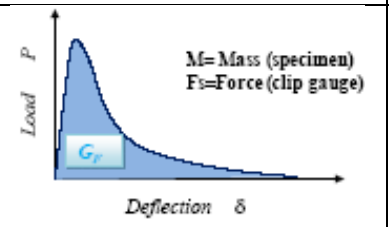
JIC-Integral	**Elastic-Plastic Materials**	$J_{IC} = \frac{2(U_e + U_p)}{B(W-a)} = \frac{2U_c}{B(W-a)}$	Uc = Total critical potential energy 3-Point SE(B) S= 4W and $0.45 \leq a/W \leq 0.65$

This method explains the propagation of cracks in low temperature below 4.4°C (40°F). In fracture mechanics, fatigue is defined as a process in which flaws in the material under repeated loading grow in size and form macro crack. The fatigue crack growth is developed in three phases. The first phase is crack initiation, second one is the crack growth and unstable crack propagation is defined as the third phase.

It is assumed that the second phase consumes most of the fatigue life and, consequently, that quantitative models based on fracture mechanics have been proposed for this phase. The

stress and strain are measured and computed based on the number of load repetitions for the second phase followed by a basic explanation (see Equation 2.4) another form for formula 2.2.

$$da/_{dN} = A(K_1)^n \quad (2.4)$$

where a = crack length, K_I= stress intensity factor in mode (stress * length/2), N= the number of load applications, and A and n are experimental coefficients. In this relation, it is assumed that the stable crack growth is occurred between some initial crack length a_I and critical length a_c which ends the fatigue life and it is determined by K_{Ic}, the critical value of K_I. The average crack speed ($da/_{dN}$) is related to the driving force through that power law equation. So the integration of equation (2.4) between initial crack length, a_0 and critical crack length, a_c gives the fatigue life.

Because the exact contributions of crack initiation and unstable crack propagation stages are not well known, the stable crack propagation stage may not explain a suitable range of the entire fatigue spectrum. As it is related to so many effective factors, it needs a lot more experimental data to use this method to evaluate the fatigue resistance of asphalt life.

2.1.7 Wheel-Tracking Testing

In full-scale wheel-track testing, a loaded wheel is used to simulate the initiation and propagation of fatigue cracking on asphalt slabs. The strains at the bottom of the slabs are measured to detect the initiation and propagation of cracks under repeated loads. These tests have also been carried out in the laboratory.

2.2 FATIGUE TESTING METHODS

Based on above testing principles there are three common and direct testing methods to evaluate the fatigue failure on asphalt mixture as (1) indirect tensile test, (2) the overlay tester (OT) and (3) the four point flexural bending method.

2.2.1 Indirect Tensile Test (ITT)

The indirect tensile strength test simulates the states of stress in the asphalt layer tension zone. It is one of the simplest methods for characterizing the asphalt concrete properties or failures caused by the tensile stresses. Figure 2.8 shows the general setup of the indirect tensile strength test and Figure 2.9 shows the schematic of load application in this method. The indirect tensile test (IDT, ASTM designation # 4123) is conducted by applying a compressive load to a cylindrical specimen through two diametrically opposed, arc shaped rigid platens. This loading configuration develops a relatively uniform state of tensile stresses perpendicular to the load direction, which results in splitting of the specimen. Tests can be conducted with a monotonic load or repeated loads for fatigue life. It can also be conducted under different test conditions such as variable temperature, moisture conditions and even different loading rates. The results are useful for determining some engineering properties to analysis the elastic or visco-elastic properties which effects on the failures such as fatigue. The IDT strength test is a suitable test to characterize the tensile strength of hot-mix asphalt (HMA), especially for thermal cracking evaluation.

The sample is placed under a diametrical repeated loading equipment (Universal Testing Machine) with Linear Variable Displacement Transducers (LVDTs) placed on both sides of the horizontal diameter to measure horizontal deformations and the load is applied diametrically to a cylindrical sample of HMA. In this method, the indirect tensile stress, σ_s, is calculated from:

$$\sigma_S = \frac{2P}{\pi dt} \tag{2.5}$$

where P = applied load; d = diameter of the specimen and t = thickness of the specimen.

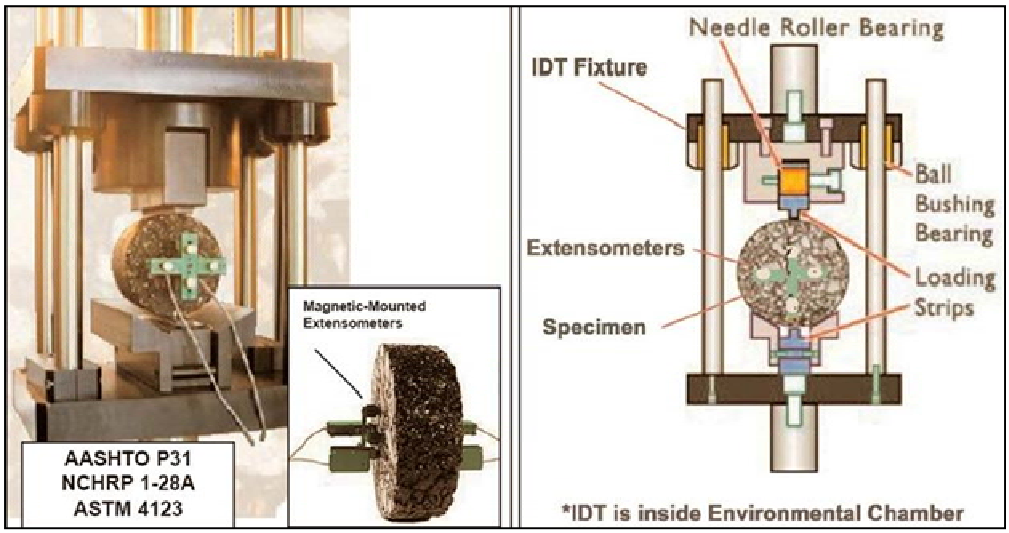

Figure 2.8 – Indirect Tensile Test Set Up

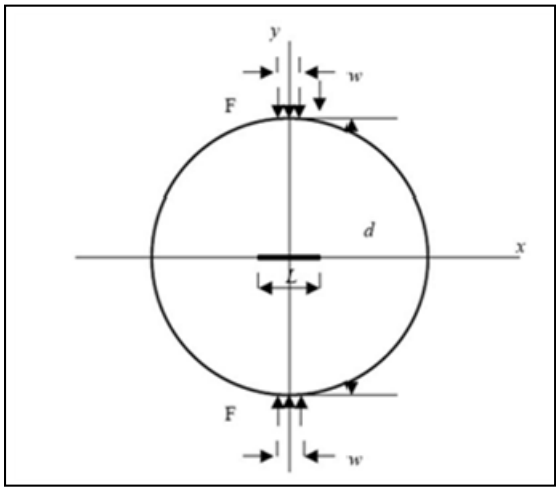

Figure 2.9 – The Schematic of Loading Application

$\sigma_S = \frac{2P}{\pi dt}$Several different models use the IDT results to predict the fatigue failure of HMA. Lee et al. (2006) proposed :

$$N_f = 14.72 \times MFIDT \times C \times f_1(\varepsilon_t)^{-f_2}|E^*|^{-f_3} \quad (2.6)$$

where N_f = number of cycles to failure, 14.72 = conversion factor between laboratory and field conditions for a thin layer, MFIDT = adjustment factor (0.3383) between beam and IDT fatigue tests, f_1, f_2, and f_3 = 0.0020, 3.6857, and 0.8723, respectively, determined from the IDT fatigue test, ε_t = tensile strain at the bottom of the AC layer, and E^* = dynamic modulus. The correction factor, C, is represented as Formula 2.7:

$$C = 10^M \quad (2.7)$$

in which :

$$M = 3.3694(\frac{V_b}{V_a+V_b} - 0.9985) \qquad M = 3.3694(\frac{V_b}{V_a+V_b} - 0.9985) \quad (2.8)$$

where V_a = air void content (%) and V_b = asphalt content (%).

2.2.2 The Overlay Tester

The TTI overlay tester was designed by Germann and Lytton, et al., (1979) to simulate the opening and closing of joints or cracks, which are the main driving force inducing reflective crack initiation and propagation. The overlay tester is used to test the asphalt specimen for reflective and fatigue cracking. Figures 2.10 and 2.11 show an updated TTI overlay tester which is able to test 6 in. (150 mm) diameter samples that could be easily fabricated in the lab using a gyratory compactor or obtained from standard field cores (Zhou and Scullion, 2004). A displacement-controlled mode is used in the overlay tester with the opening displacement of up to 2 mm (0.08 in) at 10cycles/sec. The temperature range is limited to 0–25ºC (32–77ºF).

Zhou et al. (2007) promote the Overlay Tester (OT) as a relatively new test method that is essentially a fatigue-type test in the laboratory based on the fracture mechanism.

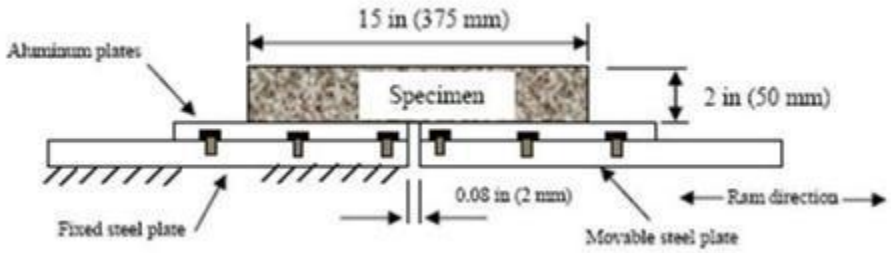

Figure 2.10 – TTI Overlay Tester Concepts

Figure 2.11 – Upgraded Overlay Tester Equipment and Sampler

The overlay tester results are used to estimate both the number of load repetitions required to form a macro-crack from micro-crack (crack initiation stage) and the number of load repetitions needed for the macro-crack to penetrate the asphalt layer (crack propagation stage). According to Zhou et al. (2006), parameters, k_2 and k_3 in Equation 2.1, of traditional fatigue model could be estimated from the fracture properties (A and n). A and n are empirically determined constants and K is stress factor or its change ΔK. These parameters are determined by measuring the crack length which can obtain from different methods. The accuracy of measurements by using different methods such as linear fracture mechanism are questionable because of the assumption used in those methods.

According to Paris' Law, the coefficient n can be defined as the inverse of stress (tensile) relaxation rate (m_t) (See 2.9).

$$n = (\frac{1}{m_t}) \tag{2.9}$$

where m_t is an exponent obtained from the tension relaxation modulus master-curve (as the slope of the log relaxation modulus versus log time graph). This measurement is valid for viscoelastic HMAC materials under a constant strained-controlled uniaxial direct-tension test. Following the Paris' Law fracture coefficient, A is a function of many parameters as Formula 2.10:

$$n = \frac{k}{\sigma_t^2 I_i}\left(\left[\frac{D_1^{(1-m_t)}E_t}{\Delta G_f}\right]^{\left(\frac{1}{m_t}\left[\frac{1}{n_{BD}+1}\right]\right)}\right)\int_0^{\Delta t} W^n(t)dt \qquad (2.10)$$

In which A is related to material coefficient (k ~0.33) , time-dependent creep compliance(D_1), elastic modulus from tension relaxation modulus master-curve (E_t in psi), repeated loading time (Δt ~0.01 s) ,surface energy due to fracture or dewetting(ΔG_f in ergs/cm^2), maximum tensile strength(σ_t), dimensionless stress integral factor in crack failure zone(I_i), brittle-ductile factor(n_{BD} , ranging between 0 and 1), load pulse shape factor($\int_0^{\Delta t} W^n(t)dt$, ranging between 0 and 1).

With known SIF (K) and crack growth rate (dc/dN), the fracture properties (A and n) can be readily determined. Figure 2.12 shows the determining of the fracture parameters (A and n) using the overlay tester (OT) for a controlled mix with a dynamic modulus of about 1500 MPa (218 ksi). Figure 2.12 also shows an example of calculating the A and n from SIF values for a selected mix (Zhou and Scullion, 2004).

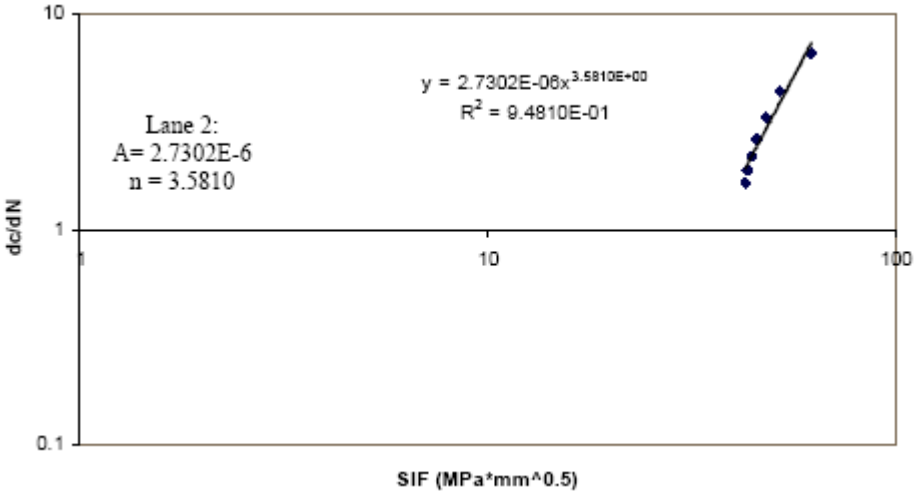

Figure 2. 12 – Example of Determining the Fracture Parameters (A and n) (Zhou and Scullion, 2004)

The approach proposed in this method is different from traditional fatigue crack approaches (such as the fatigue models used in the MEPDG) in which the fatigue crack propagation stage is not directly considered. It is also different from the often used fracture mechanics approaches which ignore the fatigue crack initiation stage. Based on theoretical derivations and experimental data, the quantitative relationships between crack initiation and crack propagation models can be developed.

Zhou et al. (2006) followed the Paris's law (Equation 2.2) to determine the stress intensity factor, SIF from

$$SIF = 0.2911 * E * MOD * c^{-0.4590} \quad (2.11)$$

E = dynamic modulus, MOD = maximum opening displacement, and c = crack length. Based on the computation of SIF, A and n data, the fatigue cracking is estimated from

$$N_f = N_i + N_p \quad (2.12)$$

where N_f = the number of traffic load repetitions to cause a crack to initiate and propagate through the asphalt surface layer, N_i = the number of load repetitions needed for micro-cracks to coalesce to initiate a macro-crack (crack initiation) and N_p = the number of load repetitions required for the macro-crack to propagate to the surface (crack propagation). Both N_i and N_p are estimated from the fracture properties (A and n), which are determined from the OT.

2.2.3 The Four-Point Bending Fatigue Test Apparatus

According to Kaloush et al. (2002) the four points fatigue asphalt beam test method is one of the most reliable methods for predicting the fatigue resistance life of asphalt mixes.

Figure 2.13 shows the schematic loading characteristics of the device used for this purpose. An asphalt concrete pavement beam is evaluated under repeated haversine or sinusoidal loading system.

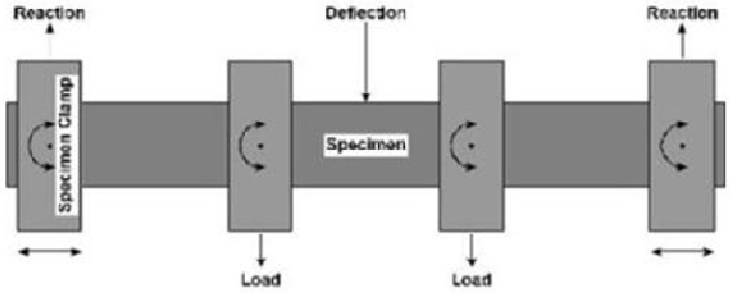

Figure 2.13 – Loading Characteristics of the Flexural Fatigue Apparatus

The existing specifications to conduct a four point bending flexural test method for an asphalt beam specimens are AASHTO T321, ASTM D7460 and SHRP M – 009. Table 2.3 includes the summary of minimum requirements for test system and some definitions for each of above specifications.

Table 2.3 – Summary of Existing Specification and the Requirements

Requirements							
Standard		**AASHTO**		**ASTM**		**SHRP**	
Designation		**T 321**		**D7460 - 08**		**M- 009**	
Load Measurement and Control	Range	0 to 4.5	KN	0 to 5	KN	±4.5	KN
	Resolution	2.5	KN	2.5	KN	0.002	KN
	Accuracy	5	KN	5	KN	±0.004	KN
Displacement Measurement	Range	0 to 5	mm	0 to 5	mm	±5	mm
	Resolution	2.5	μm	2.5	μm	0.00254	mm

and Control	Accuracy	5	μm	5	μm	±0.005	mm
Frequency Measurement and Control	Range	5 to 15	Hz	5 to 10	Hz	5 to 10	Hz
	Resolution	0.005	Hz	0.005	Hz	0.005	Hz
	Accuracy	0.01	Hz	0.01	Hz	0.01	Hz
Temperature Measurement and Control	Range	5 to 30	^{o} C	5 to 10	^{o} C	5 to 10	^{o} C
	Resolution	0.25	^{o} C	0.25	^{o} C	0.25	^{o} C
	Accuracy	0.5	^{o} C	0.5	^{o} C	±0.5	^{o} C
Fatigue Failure	Flexural Stiffness Reduction	50	%	40	%	50	%
Specimen Size	Length	380	mm	380	mm	381±6.35	mm
	Width	63	mm	63	mm	63.5±6.35	mm
	Height	50	mm	50	mm	50.8±6.35	mm

The Cox and IPC devices (see Figures 2.14 and 2.15) are two devices typically used for this test. General test conditions are limited to have the compatibility and capability to the desired constant strains 200 to 800 με and a minimum 10,000 load cycles which is suggested to get the 50% of flexural strength of specimen.

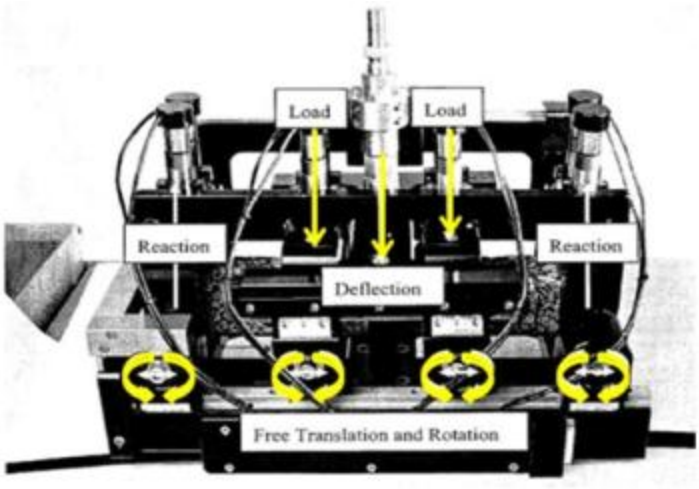

Figure 2.14 – Load and Freedom Characteristics of Fatigue Test Apparatus (Cox)

Figure 2.15 – Fatigue Test Apparatus (IPC)

2.2.4 Compaction Methods

Compaction of asphaltic concrete mixtures in flexible pavements plays a major role in the performance of these pavements. Mix properties, such as air voids are highly dependent on the degree and the method of compaction. These properties directly affect pavement performance indicators, such as rutting and fatigue cracking. Different methods such as full scale rolling wheel compaction, miniature rolling wheel compaction, and vibratory loading are recommended (Kaloush et al., 2002). Table 2.4 lists three key factors which have been identified as being important in evaluating the performance of compaction devices. The following compaction methods are available which show a good simulation between the obtained results from the site compaction.

Table 2.4 – Recommended Performance for Compaction Device (AG: PT/220, 2005)

Parameter	Performance required
Particle Orientation	To be uniform in respect to particle distribution and orientation consistent with in situ pavement materials.
Uniformity of Air Voids	Uniform distribution of air voids of specimens cut from a slab should have a mean air voids of 0.5% of the target value. The difference between maximum and minimum air voids of replicate specimens will be less than 1%.
Aggregate Crushing	There shall be no significant change in the particle size distribution of the asphalt due to the compaction process. The difference in percentage passing the 75 um sieve shall be less than 2% for measurements taken before and after the compaction process.

Kneading Compaction

Kneading compaction (ASTM D-3202) is employed in the preparation of beam specimens for fatigue testing. Compaction is achieved by repetitive loading through a tamping foot, considerably smaller in size than the specimen being compacted. During each application of the tamping foot, the load is gradually increased, maintained for a short time interval, and then released. Each subsequent loading is applied to a "fresh" portion of the exposed surface. This pattern of loading induces deformations and particle orientation similar to those which take place in situ. Walubita et al., (2004) developed a linear kneading compactor as shown in Figure 2.16 to obtain the target air voids (AV) content consistent with the specified beam thickness at a maximum compaction pressure of 6900 KPa (1000 psi).

Figure 2.16 – Linear Kneading Compactor (Walubita et al., 2004)

Beam specimens are compacted to a size of 457 mm (18 in.) length by 150 mm (6 in.) width by 63 mm (2.5 in.) thickness, and test specimens are sawn to a 380 mm (15 in.) length by 63 mm (2.5 in.) width by a 50 mm (2 in.) thickness.

Rolling Wheel Compactor

The rolling wheel method is similar to field compaction method, since the orientation of the aggregate particles and density of the mixture can closely correspond to field compaction. Figure 2.17 shows a rolling wheel compactor and Figure 2.18 the making of an asphalt beam specimen using the rolling wheel compactor. Specimen preparation can be accomplished by compacting the mixture in a large area using a roller that can impart compacting pressures similar to those which occur in the field, and then extracting the required specimens by sawing or coring from the large slabs.

Figure 2.17 – Rolling Wheel Compactor

Figure 2.18 – Compacting Asphalt using Rolling Wheel Compactor

Asphalt Vibratory Compactor Roller

The Asphalt Vibratory Compactor utilizes vibratory compression action to consolidate and compact asphalt mixtures to fabricate beam and cylindrical specimens to within a close tolerance of the target density. The compaction actions from this vibratory compaction machine closely simulate the field compaction of asphalt mixtures by the vibratory compaction roller.

Figure 2.19 shows a type of vibratory asphalt compactor. Beam mold assembly, consists of a rigid rectangular side frame, a rigid movable bottom, and two compaction plates, as shown in Figure 2.20. Standard beam specimens can be fabricated in size of 125 mm (5 in.) wide by 300 mm (12 in.) long by 75 mm (3 in.) height.

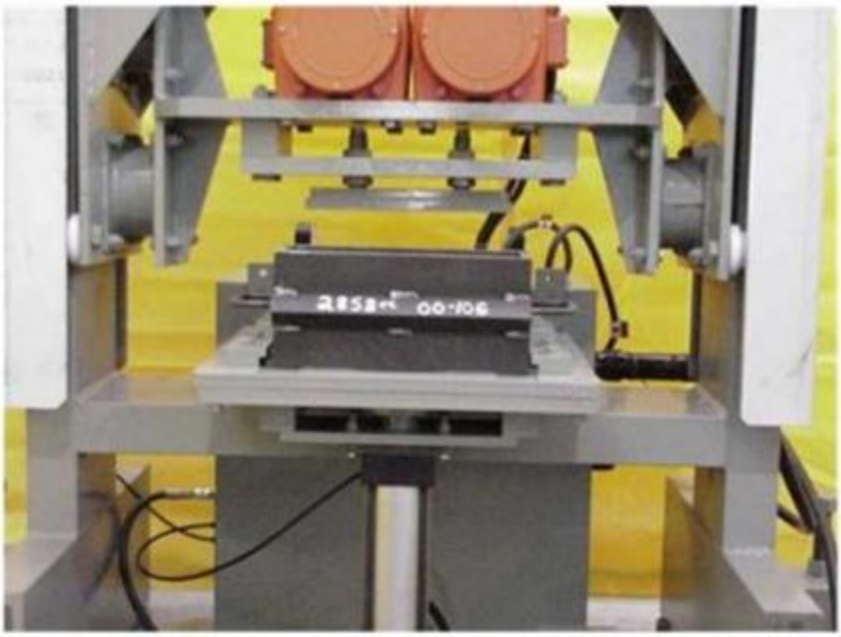

Figure 2.19 – The Vibratory Asphalt Compactor

Figure 2.20 – Mold Assembly Used to Prepare Asphalt Beam Specimen

2.2.5 Trimming

After compaction, the specimens have to be cooled to ambient temperature. The specimens are then trimmed to the required dimensions for fatigue testing by using water cooled saw to the standard dimensions as shown in Figure 2.21 (Kaloush et al. 2002).

Figure 2.21 – Specimen Sawing

CHAPTER 3

Experimental Set up

One common laboratory method for evaluating the asphalt fatigue potential is the four point bending fatigue test apparatus. In this method, a constant bending moment between two point loads is applied repeatedly to a prismatic specimen. The process followed in this study is described below.

3.1 TESTING DEVICE

A device manufactured by Industrial Process Controls Ltd. (IPC) was used to simulate the fatigue resistant life of asphalt pavement. The IPC device consists of two main related parts. One is the hardware that includes an environmental chamber, a loading cell, and a compressor. The other part is the software which interfaces to a standard beam fatigue test (BFT) loading frame (see Figure 3.1).

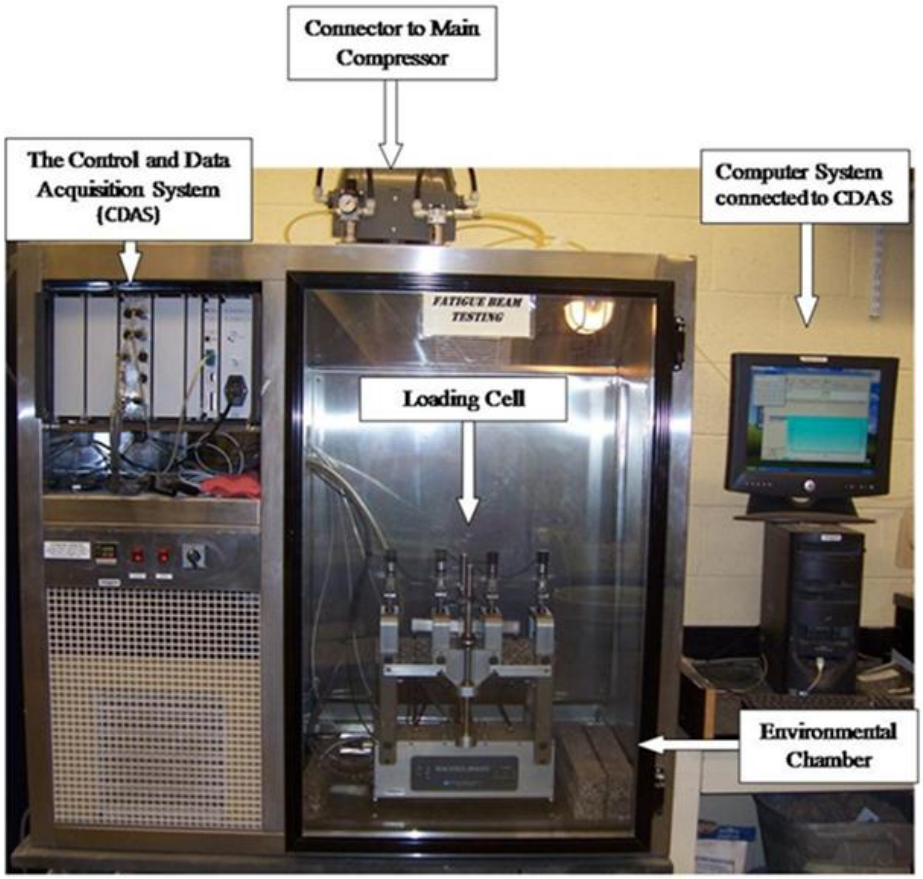

Figure 3.1 – IPC Machine Set up

Hardware

The hardware consists of three components. A control and data acquisition system (CDAS) provides servo-feedback loading control electronics, transducer data acquisition, and timing functionality. A load cell and a linear variable displacement transducer (LVDT) located in an environmental chamber (see Figure 3.2) measure or monitor the applied repeated load and displacement at the center of specimen, respectively. Load is applied to the beam through the built-in digital servo-controlled pneumatic actuator. A "floating on-specimen" transducer measures and controls the true beam deflection irrespective of loading frame compliance. A

cradle mechanism is used for free translation and rotation of the clamps that provides loading at the third points. Pneumatic actuators at the ends of the beam center the specimen laterally and also clamp it.

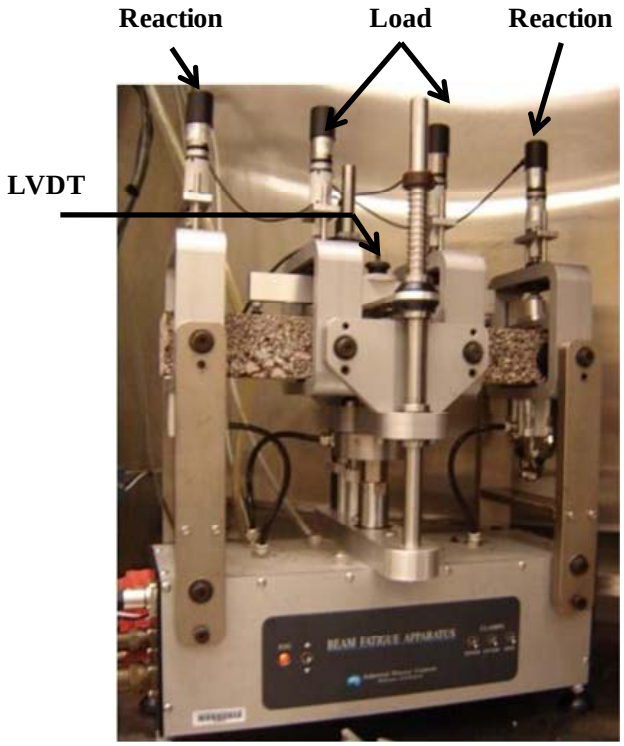

Figure 3.2 – IPC Machine Loading Cell and Components

A connector on top of the device transfers pneumatic pressure from a compressor to the load cell. Servo-motor driven clamps secure the beam at four points with a pre-determined clamping force.

The test may be controlled in either strain or stress mode, and the loading pulse wave shape is typically haversine or sinusoidal over a range of frequencies. In a stress-controlled test, the applied load is maintained and the variation in the deformation of the specimen with the number of cycles is monitored. In the stress control mode, the applied force is kept constant and the beam deflection is monitored. If any creep occurs, the minimum and maximum load levels

are adjusted to maintain a "straight" beam. Constant-strain mode, typically in the range of 200 to 800 με, was used in this study.

The environmental chamber is capable of maintaining temperature in the range of -10 ^{o}C (14 ^{o}F) and 40 ^{o}C (104 ^{o}F) with a precision of 0.5^{o}C (1 ^{o}F). In this study, tests were performed at nominal temperatures of 4.4^{o}C (40^{o}F), 21.5^{o}C (71^{o}F) and 37.5^{o}C (100^{o}F). The specimens were kept at least for 24 hrs in the environmental chamber to equilibrate them to the desired temperature. Two temperature probes were attached to the surface and core of a dummy specimen (Figure 3.3) to monitor of the test temperature.

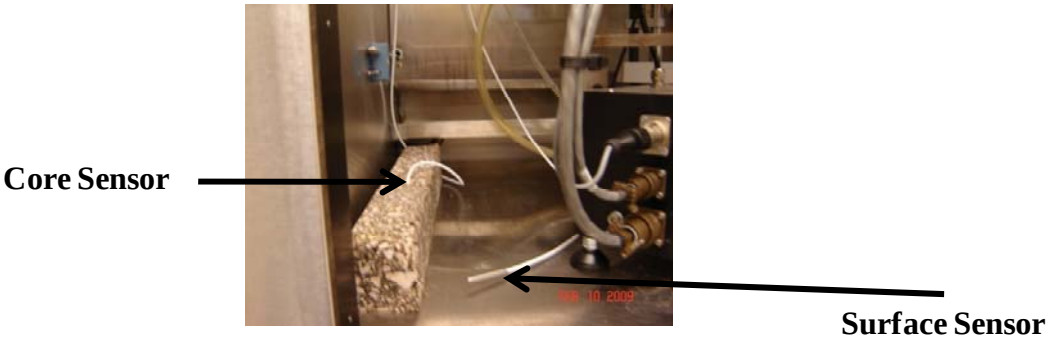

Figure 3.3 – Core and Surface Temperature Sensors

The compressor has to be capable of providing 0.4m^3/min (12 ft^3/min) of flow at the required pressure to be able of loading mechanism for the duration of a test.

Software

The software controls the data acquisition system and the servo-controlled pneumatic loading apparatus on a specimen until failure occurs. The control and data acquisition system (CDAS) provides servo-feedback loading control electronics, and transducer data acquisition and timing functionality. The software monitors the following information for each cycle of loading: (1) test duration from the start of the test (in hours, minutes and seconds), (2) number of cycles,

(3) maximum and minimum applied load (in kN), (4) maximum and minimum beam deflection (in mm), and (5) core and surface temperatures of a specimen(in ^{o}C).

A view of the software during operation is shown in Figure 3.4. Also shown is the flexural stiffness recorded during a test for each cycle as the major parameter to monitor the fatigue resistant behavior of a specimen. A file can be created to archive the test results. Alternatively, the results can be imported into a spreadsheet program for further analysis.

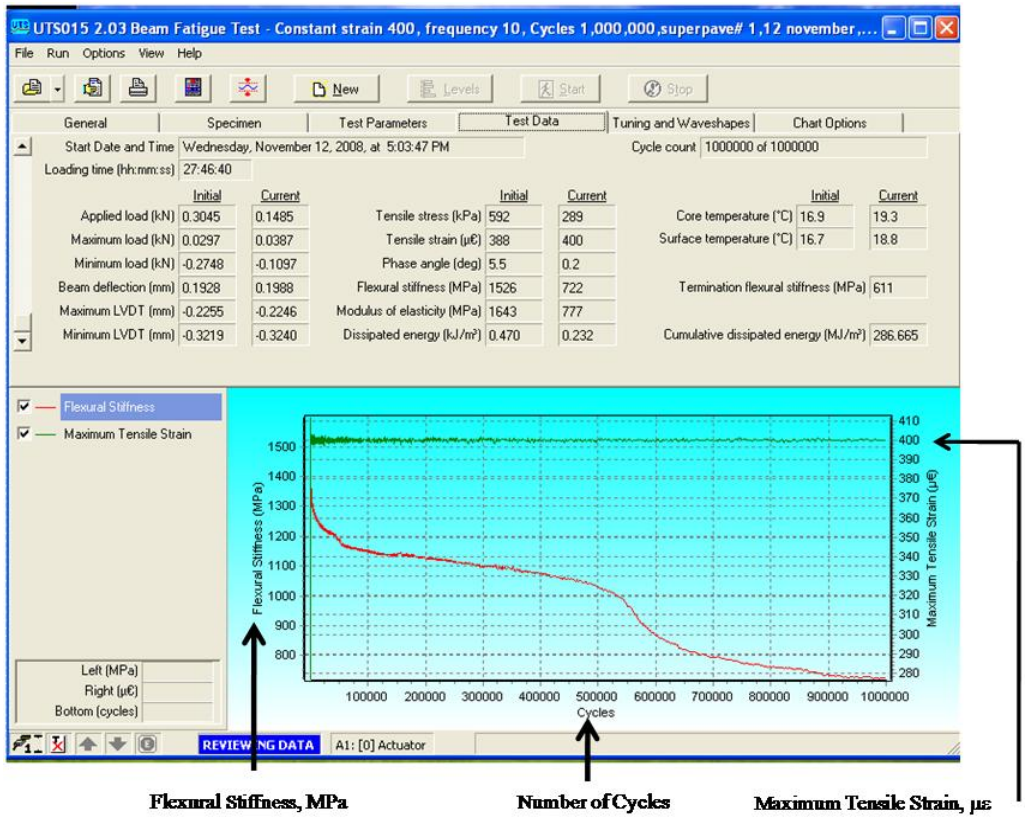

Figure 3.4 – IPC Software View While a Running Test

The software has three built-in loading programs for convenience of the user. These built-in protocols include: (1) Australian AUSTROADS AST 03:2000, (2) AASHTO T 321-03,

and (3) prEn 12697-24 advocated by the European Standard. In this research, the AASHTO specification was used.

Data Analysis

Based on the information gathered, several parameters are calculated. The tensile stress at the bottom of the specimen, σ_t, can be obtained from:

$$\sigma t = \frac{1000000 S_w P}{w h^2} \tag{3.1}$$

where S_w is Support span width (typically 356 mm), P is peak force (kN), w is average beam width (mm), and h is average beam height (mm). Similarly, the tensile strain, ε_t, is obtained from the following equation:

$$\varepsilon t = \frac{12\ \delta\ h\ 1000000}{(3S_w^2 - 4L_w^2)} \tag{3.2}$$

where δ is the peak deflection at the center of the beam (mm) and L_w is loading span width (typically 119 mm). The flexural stiffness, S, is then estimated from Formula 3.3:

$$S = \frac{1000\ \sigma t}{\varepsilon t} \tag{3.3}$$

and the phase angle, ϕ an indication of the visco-elasticity of the mix is calculated from:

$$\emptyset = 360\ f\ s \tag{3.4}$$

where f is the frequency of the applied load (typically in Hz) and s is time lag between applied load and midspan deflection (in sec). Based on the theory of elasticity, the modulus of the mix, E, is estimated from:

$$E = \left[\frac{P\ L}{\delta\ w\ h}\right]\left[\frac{(3S_w^2 - 4L_w^2)}{(4h^2)} + k^*(1+v)\right] \tag{3.5}$$

where k is the actual shear stress divided by the average shear stress (assumed 1.5) and v is Poisson's ratio (assumed as 0.4).

The damage-energy as fatigue approach is simply based on a central concept of the energy approach which is defining the energy fatigue curve. The dissipated energy, which is an indication of flexural stiffness, is calculated by determining the area within the stress-strain hysteresis loop for each captured data cycle.

Failure is defined as the number of load cycles at which this percentage of dissipated energy begins to increase rapidly, indicating instability. The number of load cycles to 50% reduction in initial stiffness was found to be highly correlated with the failure point. Using the dissipated energy concepts in fatigue analysis makes it possible to account for damage accumulation in a straightforward manner **(**Ghuzlan and Carpenter, 2006).

3.2 SAMPLE PREPARATION

Sample preparation procedures can be divided into four steps; (1) mixing, (2) compacting, (3) extracting, and (4) trimming. ASTM D7460 was followed to prepare the specimen. The nominal dimensions of the specimens were 380 mm (15 in.) in length, 63 mm (2.5 in.) in width, and 50 mm (2 in.) in height. To achieve such a size specimen, a metallic mold with the dimensions of 254 mm (16 in.) in length, 76 mm (3 in.) in width and 114 mm (4.5 in.) in height, was fabricated as shown in Figure 3.5.

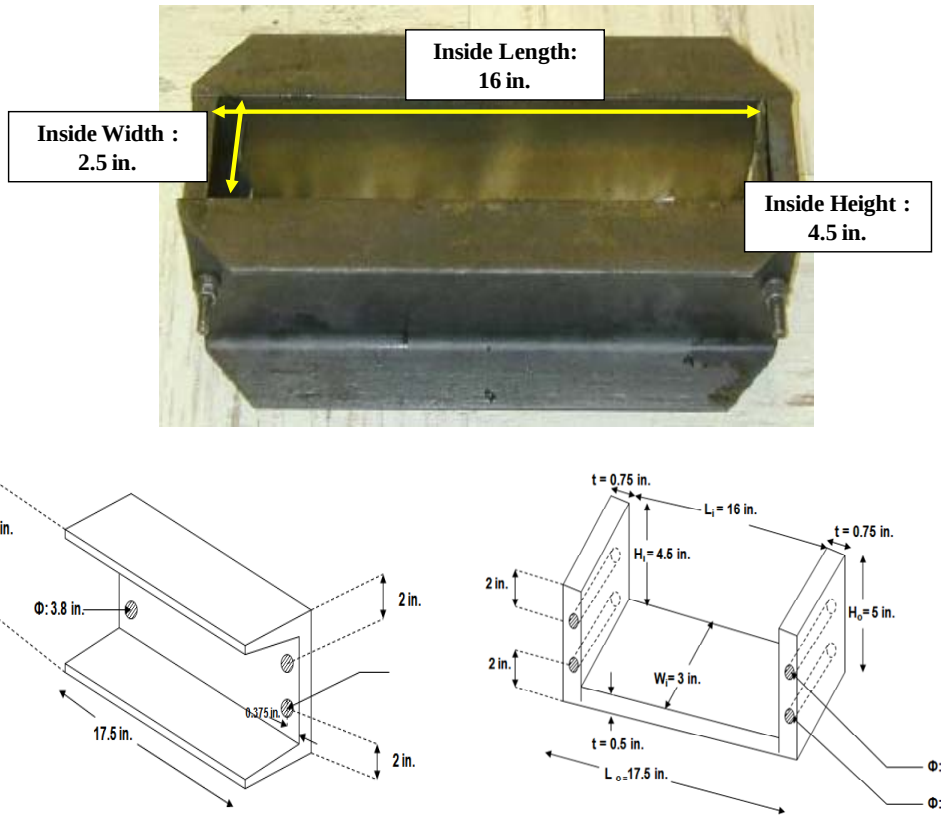

a: Mold Sides b: Mold Bottom Plates

Figure 3.5 – Mold for Preparing Beams

To apply the load uniformly to the top of the specimen, a steel plate was fabricated (see Figure 3.6). The loading plate should be rigid enough to carry the compaction load and also transfer it to the specimen.

Figure 3.7 shows the steps of preparation the mix and equipment for compaction. The amount of material necessary to achieve a nominal air void content of 7% was mixed. To prepare the specimens, the mold, loading and the asphalt mix were placed in a 177°C (350°F) oven for 3 hrs. The mix was then carefully spread in the mold uniformly.

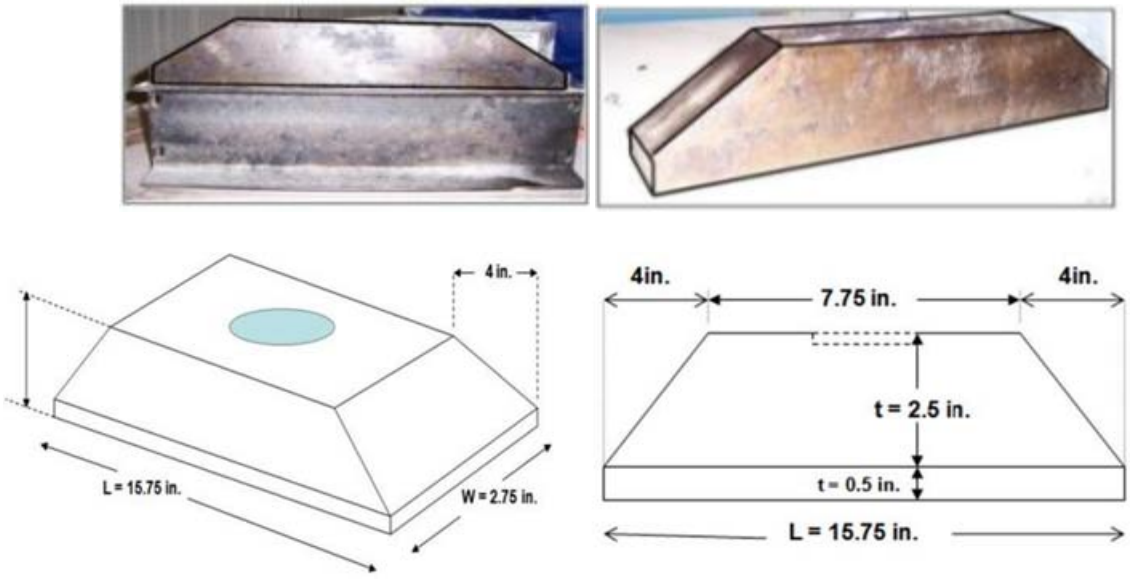

a: Side View b: Front View

Figure 3.6 – Steel Loading Plate

a : 3hrs in Oven

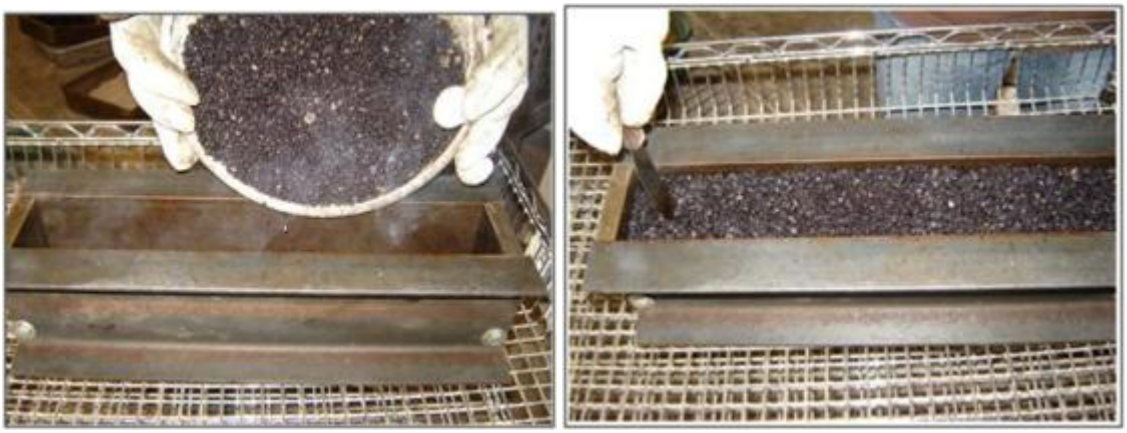

b : Pouring in the Mold

c : The Loading Lead

Figure 3.7 – Heating the Asphalt Mix and Compaction Components

An MTS device was used to compact the asphalt specimens (see Figure 3.8). To start the compaction, a 900 N (200 lb) static load was applied to the specimen (see Figure 3.8 a), followed by 500 cycles of sinusoidal loading at a rate of one cycle per seconds. The magnitude of the

sinusoidal loading was established by trial and error for each type of hot mix so that the desired height and air voids could be achieved.

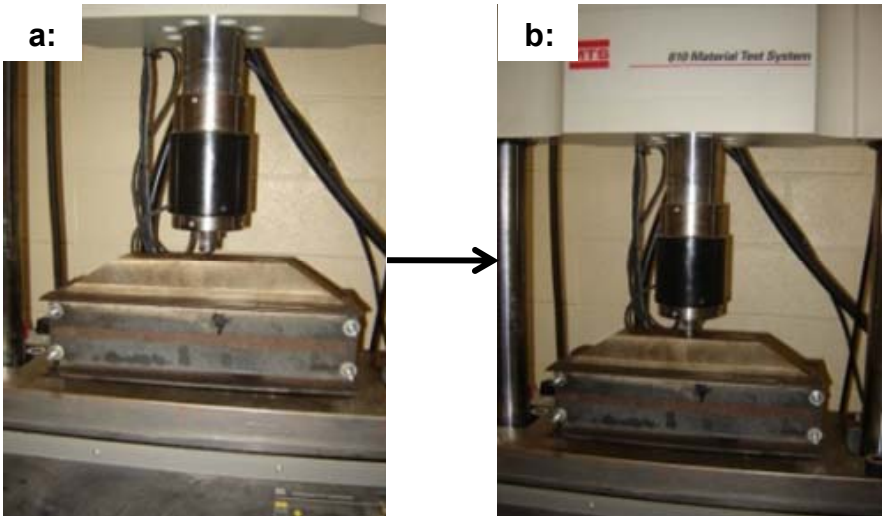

Figure 3.8 – Compaction Steps with MTS Machine

The steps involved in the extraction of the specimen consisted of removing the side plates of the mold carefully, removing the loading plate, and as the last step removing the specimen from the bottom plate, and placing it on a smooth surface to cool to room temperature (see Figure 3.9). A freshly compacted specimen is so hot and flexible that it may deform if it is extracted too early. To avoid this problem, it is necessary to wait at least 15 minutes to remove the loading plate. Figure 3.10 shows the steps for trimming the specimens. The specimens were typically trimmed a day after compaction. Figure 3.10d shows a trimmed asphalt beam.

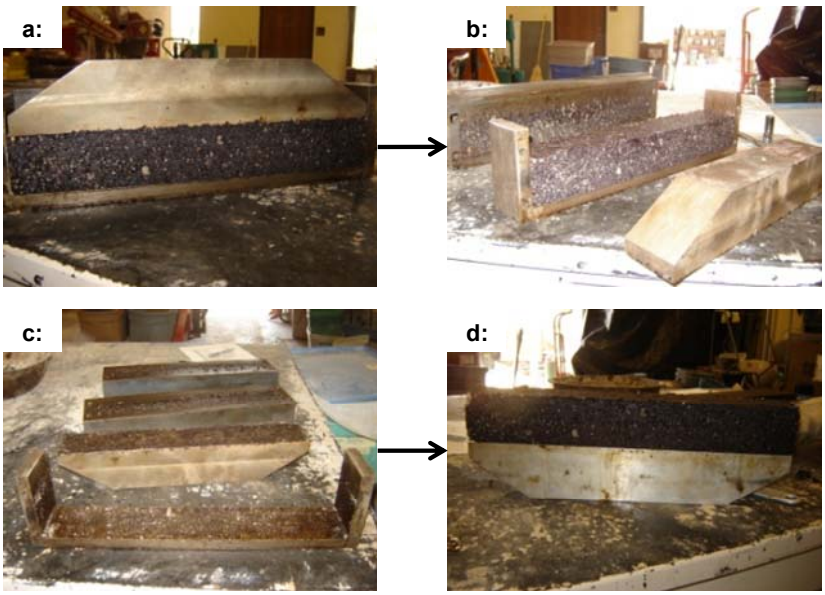

Figure 3.9 – Beam Extraction Steps

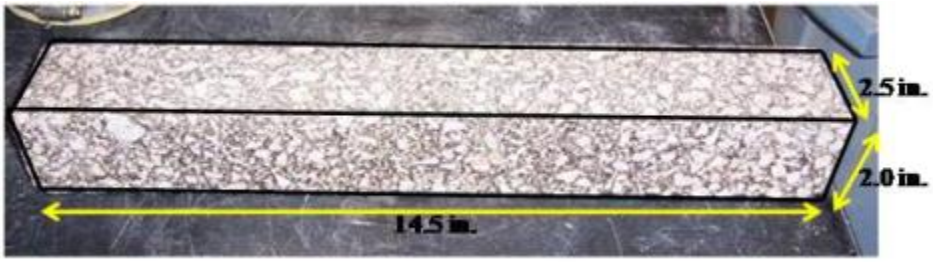

d: The Trimmed Specimen

Figure 3.10 – Trimming the Specimen to Desired Dimensions

3.3 FATIGUE TESTING

Once the beam was trimmed, the specimens were tested to characterize the air voids content and modulus of elasticity as quality control step before conducting the fatigue test. After fatigue test, the specimen mix design properties were checked as discussed below.

3.3.1 Pre-Testing Activities

Before performing the fatigue test, a series of quality control tests were carried out. These steps included ensuring the appropriate dimensions of the specimen, preliminary estimation of the closeness of the global air voids of the specimen to target air voids, and quantifying the variability of the specimen along the length and width.

Before fatigue testing, the global air voids content of a specimen was determined by weighing the specimen and dividing it by its volume to obtain the approximate bulk specific gravity. This approximate bulk specific gravity was compared with the maximum theoretical specific gravity to obtain the air voids contents. This process can be summarized in the following equations:

$$Air\ Voids = 100 * (1 - \frac{W_{maesured}}{W_{max}}) \quad (3.6a)$$

$$W_{\max=} V \times G_{mm} \times \gamma_w \quad (3.6b)$$

$$Air\ Voids = 100(1 - \frac{G_{mb}}{G_{mm}}) \quad (3.2a)$$

where $W_{measured}$ is the weight of the specimen, W_{max} can be calculated V is specimen volume, G_{mm} is maximum bulk specific gravity of asphalt mix and γ_w is the unit weight of water (assumed 9.8 kN/m^3, 62.4 lb/ft^3). If this value was different by more than 2% of the target value, the specimen was discarded.

Table 3.1 includes an example of the results for a Type D specimen before and after trimming. The air voids for specimen before trimming is 10.6% and after trimming is 8.8% demonstrating the importance of trimming process.

Table 3. 1– The Initial Air voids Content Estimation of Compacted Specimen – Type D

Specimen	Average Dimensions			Volume, m^3	Maximum Weight, Kg	Measured Weight, Kg	Air Voids, %	Density, Kg/m^3
	Length, mm	Height, mm	Width, mm					
Before Trimming	433.9	58.8	69.9	1.8	4.297	4.018	10.6	2232
After Trimming	414.5	55.5	66.3	1.5	3.581	3.413	8.8	2275

3.3.2 Fatigue Testing

Figure 3.11 shows the set up of the specimen. The clamps were used to fix the specimen and mark the loading points on the top for measuring (Figure 3.11a). The loading points for each specimen were done before running each test. After fixing the specimen, the clamps were released to give a free displacement to the specimen under the loading (Figure 3.11b).

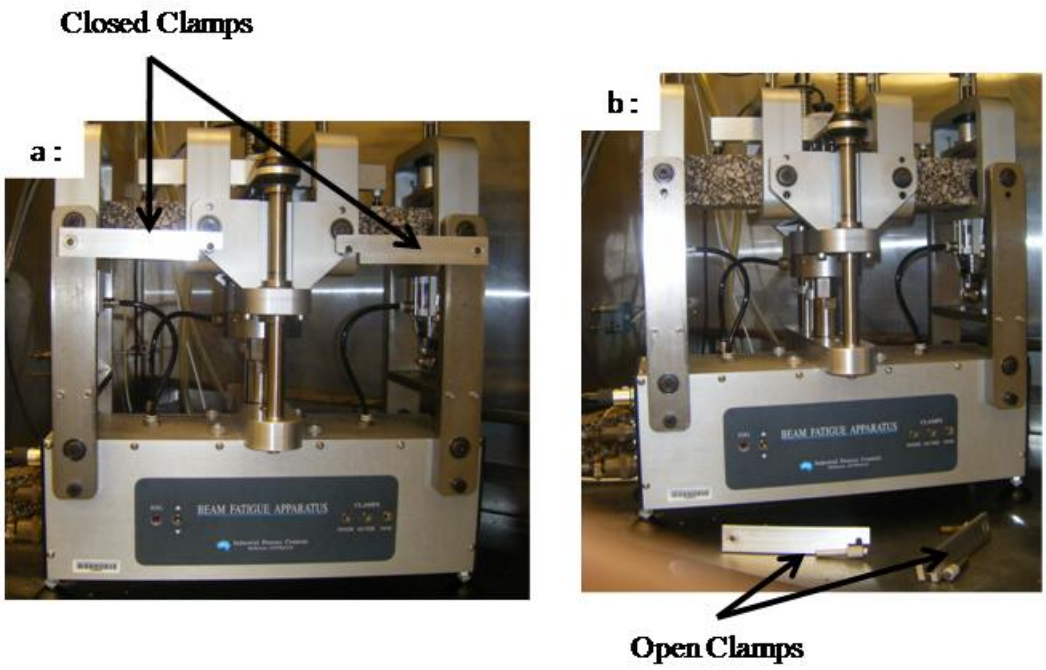

Figure 3.11 – Running Fatigue Test in IPC Machine

Figure 3.12 shows the preview of an example report after the fatigue test for a Type D specimen at a 21.5 ^{o}C (70.7 ^{o}F) temperature. The desired air voids content was supposed to be 7%. A strain of 400 με was used with a loading frequency of 10 Hz. The initial (after 50th cycle of loading) flexural stiffness and modulus of elasticity were 1492 MPa and 1613 MPa, respectively.

FileName: C:\Documents and Settings\smontazeri\Desktop\IPC_Program\Data\Asphalt Specimen\Type D-36 Kips\4.4 T-Type D-36Kip\4.4T-4(

Test Method: AASHTO Designation: T 321-03 Determining the Fatigue Life of Compacted Hot-Mix Asphalt (HMA) Subjected to Repeated Flexural Bending
Project: Asphalt Specimen -
Operator: S1
Comments: Constant strain 400, frequency 10, Cycles
1,000,000,4.4T,12 december,36K,with out clamps

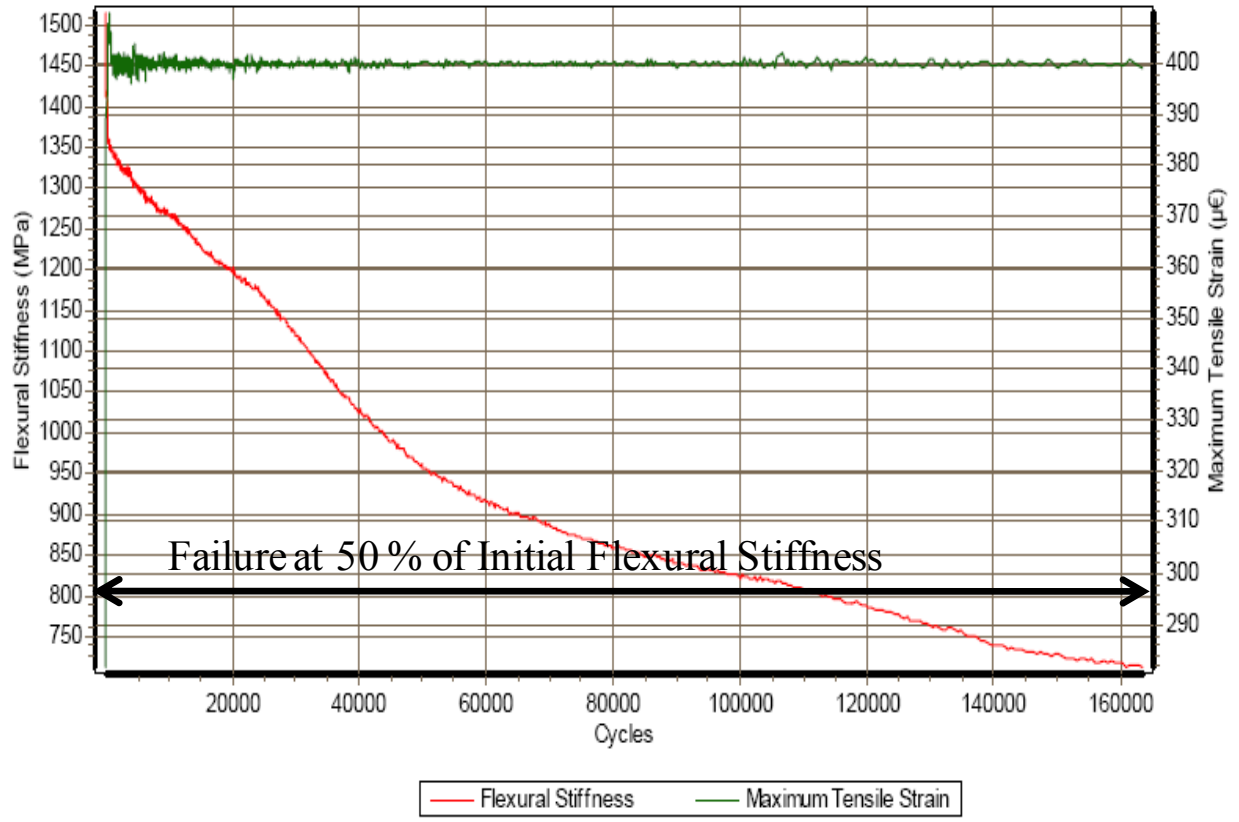

Test Data

Start Date and Time: Friday, December 12, 2008, at 10:08:41 AM
Cycle count: 163420 of 1000000
Loading time (hh:mm:ss): 04:32:22

	Initial	Current		Initial	Current		Initial	Current
Applied load (kN):	0.3176	0.1636	Tensile stress (kPa):	552	284	Core temperature (°C):	5.8	4.3
Maximum load (kN):	0.0868	0.0930	Tensile strain (με):	370	399	Surface temperature (°C):	3.1	3.1
Minimum load (kN):	-0.2309	-0.0706	Phase angle (deg):	5.2	-1.5			
Beam deflection (mm):	0.1787	0.1927	Flexural stiffness (MPa):	1492	712	Termination flexural stiffness (MPa):	597	
Maximum LVDT (mm):	-0.2227	-0.2181	Modulus of elasticity (MPa):	1613	770			
Minimum LVDT (mm):	-0.3121	-0.3145	Dissipated energy (kJ/m³):	0.412	0.231	Cumulative dissipated energy (MJ/m³):	44.256	

Figure 3.12 – Summary Report for Type D

3.3.3Post-Testing Activities

Following each fatigue test, each asphalt beam was cut in to three pieces. The air voids contents and modulus of elasticity of each piece was measured. Table 3.2 includes the air voids. As the air voids obtained from Gmb method for Superpave and Type D specimens were off, the Gmb method was not done for this specimen.

Table 3. 2– Air Voids Contents by G_{mb} Method

Section	Air Voids, %
1	5.2
2	8.6
3	7.1

V-Meter Test Method

The variability of the specimen was also evaluated using an ultrasonic device, called a V-meter (ASTM C-597, see Figure 3.13). The V-meter is an ultrasonic device that measures the travel time of compressive waves that can be translated to the modulus of elasticity of the material using:

The V-meter is an ultrasonic device that measures the travel time of compressive waves that can be translated to the modulus of elasticity of the material using:

$$E = \rho \times V_c^2 \times \frac{(1-\mu)}{(1+\mu)\times(1-2\mu)} \quad (3.3a)$$

where E is the dynamic elastic modulus, ρ is the density, μ is the Poisson's ratio of mix, and V_c is the wave velocity.

a: Top and Bottom Sides b: Back and Front Sides

Figure 3.13 – V-Meter Testing

With this device, the variations in the modulus of the specimen along the length in two directions (from side-to-side and from top-to-bottom) were measured at 4 points. The top to bottom moduli are slightly lower than the side-to-side moduli. As an example Table 3.3 is shown the design moduli calculated based on the travel times through the different sides of specimens using V-meter device for a Superpave specimen, with 7% air void design target.

Table 3. 3 – Design Modulus Data, Obtained from Ultrasonic Method

Section	**Design Modulus, ksi**	
	Back and Front Sides	**Top and Bottom Sides**
1	868	899
2	929	988
3	925	953

3.4 EXPERIMENTAL DESIGN

The goals of this study were to reveal the performance of four-point bending machine (IPC) to test different asphalt mix behavior under the cyclic loading and controlled test conditions. The available device (IPC) sets up fixed test conditions of loading and environmental conditions to simulate precisely the wheel loading effects on asphalt pavement during its life time duration. To fulfill these goals, a number of specimens were prepared and tested. The following experimental design was followed for material selection and parametric study.

Parametric Study

A number of parameters as discussed below were studied. The range and justification for each parameter are provided.

3.4.1 Repeatability

To evaluate the reliability of the obtained results from IPC machine, a synthetic specimen and several mixes were tested in triplicate. The repeatability study was done for an applied strain of 400 με at a loading frequency of 10 Hz, and a temperature of 21.5 ^{o}C (70.7 ^{o}F). The nominal selected air voids for the material was 7%.

3.4.2 Frequency of Loading

The loading frequency should change the stiffness of the specimen which may impact the fatigue life of the mix. Three loading frequencies of 5 Hz, 10 Hz, and 15 Hz, were selected based on the capabilities of the IPC and the practicality of testing.

3.4.3 Temperature Variation

To investigate the fatigue life of a specimen as a function of its viscoelasticity, the effects of temperature have to be considered. Tests were carried out at three different temperatures of 4.4 ^{o}C (39.9 ^{o}F) , 21.5 ^{o}C (70.7 ^{o}F) and 37.5 ^{o}C (99.5 ^{o}F) to consider these effects.

3.4.4 Strain Variation

The thickness and the modulus of the base layer impacts the strain experienced by the hot mix asphalt. The strains of 200, 400 and 600 με were selected for this purpose.

3.4.5 Air voids Variation

Determination of the effects of air-void and asphalt contents on laboratory fatigue life and flexural stiffness is a necessary first step in determining their effects on in-situ pavement performance. Three different air voids contents of 4%, 7%, and 11% were selected.

3.5 MATERIAL SELECTION

The same asphalt binder and aggregate source were used for the selected mixes. A granite aggregate commonly used in El Paso was used. The stiffness of binder was PG 76- 22. Four mix types namely Type D (a fine-grained mix), Superpave-C and CMHB-C (two medium-coarse mixes) and PFC (a coarse-grained mix) were used. The job mix formulas of these mixes are shown in Table 3.4.

Table 3. 4 – Mix Design for Used Material (Reyes et al., 2008)

Property		(El Paso) Red Granite			
		CMHB	**Superpave**	**PFC**	**Type-D**
Binder Grade		**PG 76- 22**			
Binder Content,%		**5.3**	**4.8**	**6.6**	**5.1**
Sieve Size, in.	**Sieve No.**	**Percent Passing, %**			
1		100	100	100	100
0.75	**(3/4)**	99	99	100	100
0.492	**(1/2)**	78.5	95	90	99
0.375	**(3/8)**	60	92.5	47.5	92.5
0.187	**(No. 4)**.	5	77.5	10.5	60
0.0929	**(No. 8)**	2	43	5.5	38
0.0469	**(No. 16)**	16	30	5	27
0.0234	**(No. 30)**	-	-	4.5	21
0.0117	**(No. 50)**	-	-	3.5	13.5
0.0029	**(No. 200)**	7	6	2.5	4.5
Maximum SG		2.471	2.520	2.469	2.497
Aggregate Bulk SG		2.601	2.655	2.526	2.696
Binder SG		**1.02**			
AV at Ndesign=100,%		4.0	4.0	20.0	4.0
VMA at Ndesign=100, %		13.7	13.2	27	15.5
VFA at Ndesign=100,%		69.7	69.9	25.8	74.2
Effective Asphalt Content, %		4.1	3.9	3.6	4.0
Dust Proportion		1.3	1.3	0.4	1.1

Table 3.5 contains the results of supplementary test carried out on the mixes.

Table 3. 5– Summary Results from Supporting Tests (Reyes et al., 2008)

Mix Type	Test			
	Dynamic Modulus at 10 Hz, MPa	**Tensile Strength at Failure, kpa**	**Maximum Strain after 10,000 sec, μ-mm./mm**	**Hamburg Wheel Tracking Device**
CMHB	5840	779	5280	958
Superpave	4785	800	4860	910
PFC	1331	421	7150	345
Type D	6088	814	3683	*

. **Test was not performed for Type D*

CHAPTER 4

Presentation of Results

Based on the tests performed in this study, the repeatability of fatigue test apparatus, and the impacts of frequency, applied strain, and temperature for four mixes were assessed. The impact of air voids was also studied for three mixes. Typically, tests were repeated five times on a synthetic specimen and in triplicates on the HMA mixes.

The results from the Superpave mix are used as examples in this chapter. Comprehensive results are provided in Appendix B for all mixes and Appendix C for synthetic specimen.

4.1 REPEATABILITY

Table 4.1 contains the summary of the results obtained for a synthetic specimen tested five times at a strain of 400 με, a temperature of 21.5^{o}C and a frequency of 10 Hz. The device is extremely repeatable as judged with coefficients of variations of less than 1% among the five repeats. Figure 4.1 shows the variations in the flexural stiffness with the number of cycles for the five trails. The source of small fluctuations in the results from the fifth trial can be attributed to the inadequacy of the compressor used initially. As a result of this study, a higher output compressor was used from then on.

The results from repeatability tests of the three Superpave specimens are shown in Table 4.2. The specimens were tested at a strain of 400 με, a temperature 21.5 ^{o}C and a frequency of 10 Hz. The results are once again reasonably repeatable with a maximum COV of about 9% for stiffness reduction. This level of variability is supported by the 5.5% COV of air voids.

Table 4.1 – Repeatability Results for Synthetic Specimens

Trial No.	Flexural Stiffness, MPa		Flexural Stiffness Reduction, %	Modulus of Elasticity, MPa	
	Initial	Final		Initial	Final
1	1069	1067	0	1139	1137
2	1062	1069	0	1132	1139
3	1072	1069	0	1142	1139
4	1077	1072	0	1148	1142
5	1071	1073	0	1141	1143
Average	1070	1070	0	1140	1140
COV, %	0.5	0.2	-	0.5	0.2

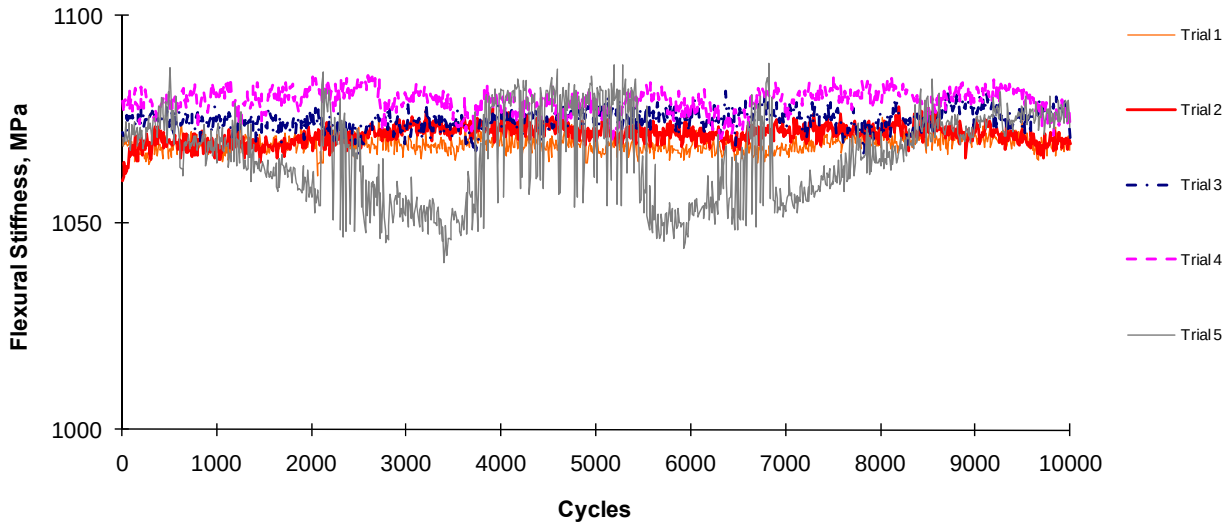

Figure 4.1 – Repeatability Results for Synthetic Specimens

Table 4.2 – Repeatability Results for Superpave Specimens

Specimen	Air Voids Content, %	Flexural Stiffness, MPa		Flexural Stiffness Reduction,%	Modulus of Elasticity, from IPC, MPa		Ultrasonic Modulus, MPa	
		Initial	Final		Initial	Final	Average	COV, %
1	7.2	1259	889	29.4	1362	961	4907	3.3
2	6.8	1343	1013	24.6	1439	1085	4527	5.8
3	6.5	1330	977	26.5	1430	1051	4310	2.5
Average	6.8	1311	960	26.8	1410	1032	4581	3.8
COV, %	5.1	3.5	6.6	9.0	3.0	6.2	6.6	-

The ultrasonic moduli reported in the table correspond to six measurements along the length of the specimens with the v-meter. Three measurements corresponded to the top-to-bottom measurements (along the height) and three to side-to side measurements (along the width). The COV of these measurements is as high as 5.8% indicating that the compaction of the specimens was carried out reasonably uniformly. The overall COV of the moduli of the three specimens are 6.6% which indicates that the three specimens are reasonably similar.

Table 4.3 contains the summary of the repeatibality study for all four mixes. The two finer mixes (Superpave and Type-D) exhibited greater reduction of flexural stiffness as compared to the two coarser mixes (CMHB and PFC), even though the two fine mixes demonstrated higher moduli. Even though before trimming, all specimens exhibited similar air voids, after trimming some variations in the air voids are evident. For the Type-D and CMHB mixes the COV of the air voids is greater than 15%. These large variations in the air voids are not observed in the initial and final flexural stiffness or the moduli of the specimens. As such,

aside from experimental error, the large variations in the air voids can be attributed to the difficulties in measuring the air voids of these specimens.

Table 4.3 – Summary of Repeatability Results of All Mixes

Mix Type	Values	Air voids, %	Flexural Stiffness, MPa		Flexural Stiffness Reduction, %	Modulus of Elasticity, from IPC, MPa		Ultrasonic Modulus, MPa	
			Initial	Final		Initial	Final	Average	COV, %
Superpave	Average	6.8	1311	960	26.8	1410	1032	4581	3.8
	COV, %	5.1	3.5	6.6	9.0	3.0	6.2	6.6	-
Type D	Average	6.4	1136	858	24.2	1222	948	4267	5.4
	COV, %	24.2	7.5	4.3	18.7	7.5	7.1	16.4	-
CMHB	Average	5.9	1223	1037	15.1	1303	1105	3719	7.5
	COV, %	15.2	4.6	3.6	27.0	4.6	3.4	5.6	-
PFC	Average	15.6	1094	957	12.3	1165	1019	1821	6.3
	COV, %	3.6	6.4	8.7	70.7	6.1	8.4	8.9	-

A careful review of the flexural stiffness reduction indicates much higher variability in this parameter as compared to the intial or final flexural stiffness. This parameter contains higher uncertainty because of the accumulation of the uncertainties in the initial and final flexural stiffnesses.

4.2 FREQUENCY VARIATION

The synthetic specimen was tested at 10, 15, and 20 Hz loading frequencies. As reflected in Appendix C, the results were practically independent of the frequency of loading.

The four mixes were then tested at loading frequencies of 5, 10, and 15 Hz. The detailed results are provided in Appendix B, and the summary results are shown in Table 4.4. The impact of the frequency on the measured parameters in the range of frequencies of 5 to 15 Hz is rather small and within the magnitude of uncertainties anticipated due to variations in the uniformity of the specimens.

Table 4.4 – Summary of Frequency Results of All Mixes

a- Flexural Stiffness

Mix Type.	Flexural Stiffness, MPa											
	5 Hz				10 Hz				15 Hz			
	AV, %	Initial	Final	Reduction, %	AV, %	Initial	Final	Reduction, %	AV, %	Initial	Final	Reduction, %
Superpave	6.6	1508	1043	30.8	6.8	1410	1013	28.2	6.4	1398	882	36.9
Type D	5.8	1238	896	27.7	7.3	1234	879	28.8	6.9	1446	981	32.2
CMHB	7.0	1111	1005	9.5	5.9	1219	1078	11.6	5.9	1076	913	15.1
PFC	17.8	1113	1015	8.8	16.2	1021	905	11.4	13.5	1166	1049	10.0

b- Modulus of Elasticity

Mix Type	5 Hz				10 Hz				15 Hz			
	Modulus of Elasticity, MPa											
	IPC		V-Meter		IPC		V-Meter		IPC		V-Meter	
	Initial	Final	Average	COV, %	Initial	Final	Average	COV, %	Initial	Final	Average	COV, %
Superpave	1621	1121	4749	6.0	1511	1085	4527	5.8	1497	944	4317	3.4
Type D	1334	965	4002	4.1	1328	1018	4504	3.6	1556	1056	4610	6.1
CMHB	1182	1070	3557	7.9	1297	1147	3694	7.0	1150	976	3571	6.8
PFC	1180	1076	1782	11.2	1093	968	1647	6.2	1240	1116	1904	5.7

As reflected in Figure 4.2, the reduction in the flexural stiffness either increases slightly or stays the same for all mixes.

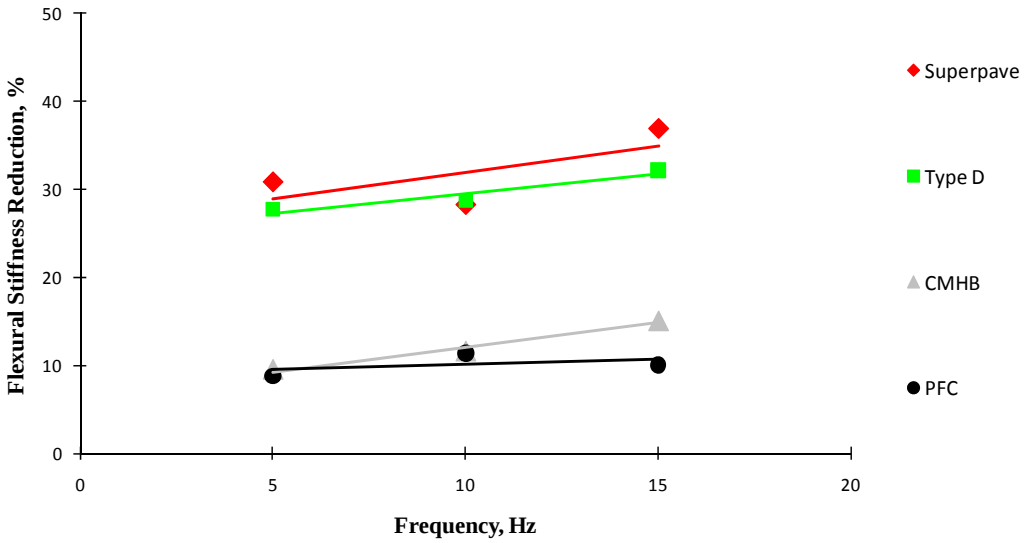

Figure 4.2 – Frequency Variations Results for All Types

4.3 STRAIN VARIATIONS

The loading strain was varied between 200 με and 600 με. Table 4.5 contains the summary of the tests results for all four mixes. The detailed results are contained in Appendix B. Even though not reflected in the initial flexural stiffnesses, as the strain level is increased the flexural stiffness reduction increased. As reflected in Figure 4.3, in many cases, the rate of flexural strength reduction is significantly greater between 400 με and 600 με levels than 200 με to 400 με levels.

Table 4.5 – Summary of Strain Variation Results of All Mixes

a- Flexural Stiffness

Mix Type	Flexural Stiffness, MPa											
	200 με				400 με				600 με			
	AV, %	Initial	Final	Reduction, %	AV, %	Initial	Final	Reduction, %	AV, %	Initial	Final	Reduction, %
Superpave	6.1	1695	1321	22.1	6.8	1410	1013	28.2	6.0	1124	557	50.4
Type D	7.4	1340	1196	10.8	7.3	1234	879	28.8	6.5	984	669	32.1
CMHB	5.8	1107	1034	5.9	11.6	1219	1078	11.6	6.0	1279	1064	16.8
PFC	16.1	1060	1052	0.8	17.5	1021	905	11.42	18.2	967	872	9.8

b- Modulus of Elasticity

Mix Type	200 με				400 με				600 με			
	Modulus of Elasticity, MPa											
	IPC		V-Meter		IPC		V-Meter		IPC		V-Meter	
	Initial	Final	Average	COV, %	Initial	Final	Average	COV, %	Initial	Final	Average	COV, %
Superpave	1822	1420	4843	2.3	1511	1085	4527	5.8	1202	596	4967	2.2
Type D	1427	1273	4858	2.6	1131	961	4820	5.2	1063	722	4070	6.7
CMHB	1183	1105	3644	6.6	1297	1147	3694	7.0	1357	1129	3690	4.7
PFC	1124	1116	2205	8.2	1093	968	1647	6.2	1032	930	1821	1.7

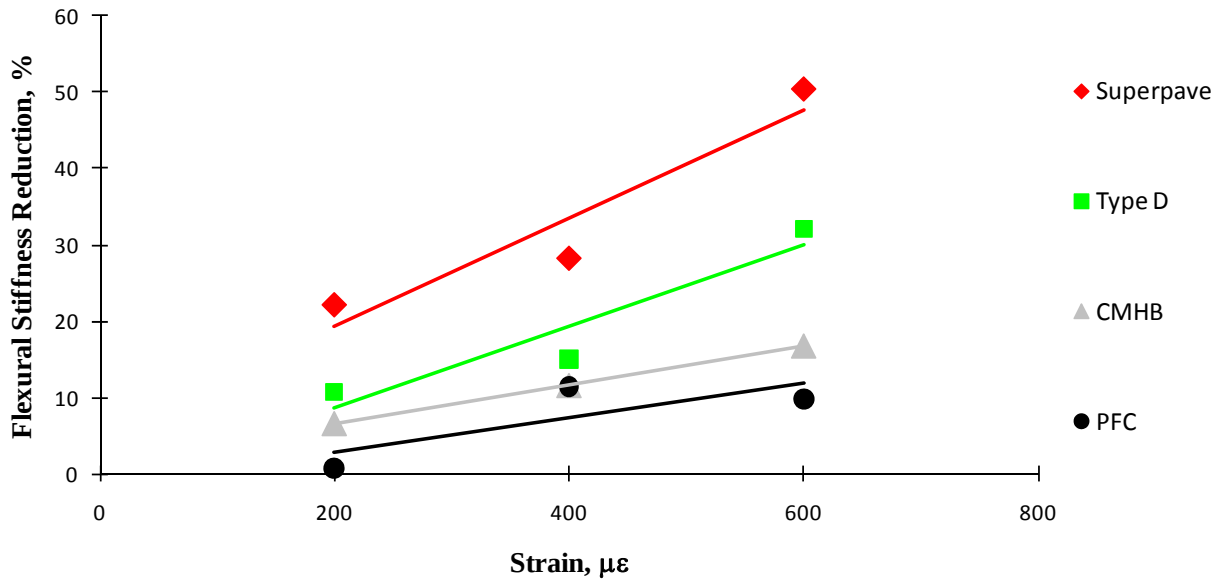

Figure 4.3 – Strain Variations Results for All Mixes

4.4 TEMPERATURE VARIATIONS

The synthetic specimen was tested at three different temperatures of 4.4°C, 21.5 °C and 37.5 °C. As shown in Appendix C, the impact of decreasing in temperature was significant, which at 4.4°C where the big variations in the flexural strength reduction were observed.

As shown in Table 4.6 for the four mixes, as the temperature increases the initial flexural stiffness decreases. This trend is anticipated. The flexural stiffness reduction is also significantly impacted by the temperature for all mixes as shown in Figure 4.4. However, the PFC mixes are less influenced by the change in temperature. For the other three mixes, the specimens did not survive the 1 million cycle of loading as shown in Appendix B.

Table 4.6 – Summary of Temperature Variations Results of All Mixes

a- Flexural Stiffness

Mix Type	Flexural Stiffness, MPa											
	4.4 °C				21.5 °C				37.5 °C			
	AV, %	Initial	Final	Reduction, %	AV, %	Initial	Final	Reduction, %	AV, %	Initial	Final	Reduction, %
Superpave	7.0	2411	1385	42.5	6.8	1410	1013	28.2	5.7	926	836	9.7
Type D	7.7	1492	712	52.2	6.9	1054	896	15.0	5.2	880	820	6.9
CMHB	6.2	1600	803	49.8	5.0	1168	1005	14.0	7.0	910	853	6.2
PFC	15.7	1166	1011	13.3	16.2	1021	905	11.4	16.2	922	896	2.8

b- Modulus of Elasticity

Mix Type	4.4 °C				21.5 °C				37.5 °C			
	Modulus of Elasticity, MPa											
	IPC		V-Meter		IPC		V-Meter		IPC		V-Meter	
	Initial	Final	Average	COV, %	Initial	Final	Average	COV, %	Initial	Final	Average	COV, %
Superpave	2579	1482	4641	9.1	1511	1085	4527	5.8	985	890	4373	5.2
Type D	1613	770	4287	3.9	1131	961	4942	5.2	940	875	4338	2.6
CMHB	1702	854	4220	2.8	1246	1071	3937	8.8	969	909	3656	5.4
PFC	1250	1084	2606	4.1	1093	968	1647	6.2	982	954	2237	11.2

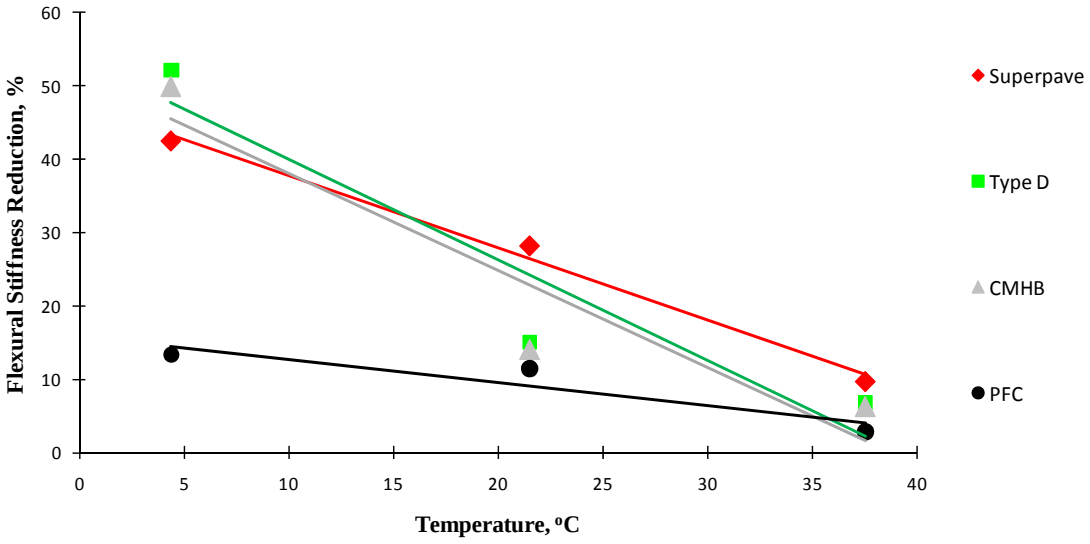

Figure 4.4 – Temperature Variations Results for All Mixes

4.5 AIR VOIDS VARIATIONS

The impact of air voids was studied for the Superpave, Type D, and CMHB mixes. Table 4.7 and Figure 4.5 show the summary of the results. For each mix type, the higher the air voids content is, the greater the reduction in flexural stiffness will become. For all mixes the initial flexural stiffness is greater for the medium air voids as compared to the low and high air voids.

Table 4.7 - Summary of Air Voids Variations Results of All Mixes

a- Flexural Stiffness

Mix Type	Flexural Stiffness, MPa											
	Low				Medium				High			
	AV, %	Initial	Final	Reduction, %	AV, %	Initial	Final	Reduction, %	AV, %	Initial	Final	Reduction, %
Superpave	5.9	1171	961	17.9	6.8	1410	1013	28.2	7.5	1169	742	36.5
Type D	4.5	1278	1110	13.1	5.8	1208	1017	15.8	7.3	1234	879	28.8
CMHB	4.0	1138	1001	12.0	6.8	1280	1030	19.5	8.5	1153	1003	13.0

b- Modulus of Elasticity

Mix Type	Modulus of Elasticity, MPa											
	Low				Medium				High			
	IPC		V-Meter		IPC		V-Meter		IPC		V-Meter	
	Initial	Final	Average	COV, %	Initial	Final	Average	COV, %	Initial	Final	Average	COV, %
Superpave	1248	1032	5199	8.8	1511	1085	6547	5.8	1245	791	5902	3.6
Type D	1358	1180	4759	4.4	1288	1085	4504	3.6	1328	1018	3615	6.0
CMHB	1213	1067	2730	9.1	1365	1099	3526	6.5	1229	1070	3877	7.0

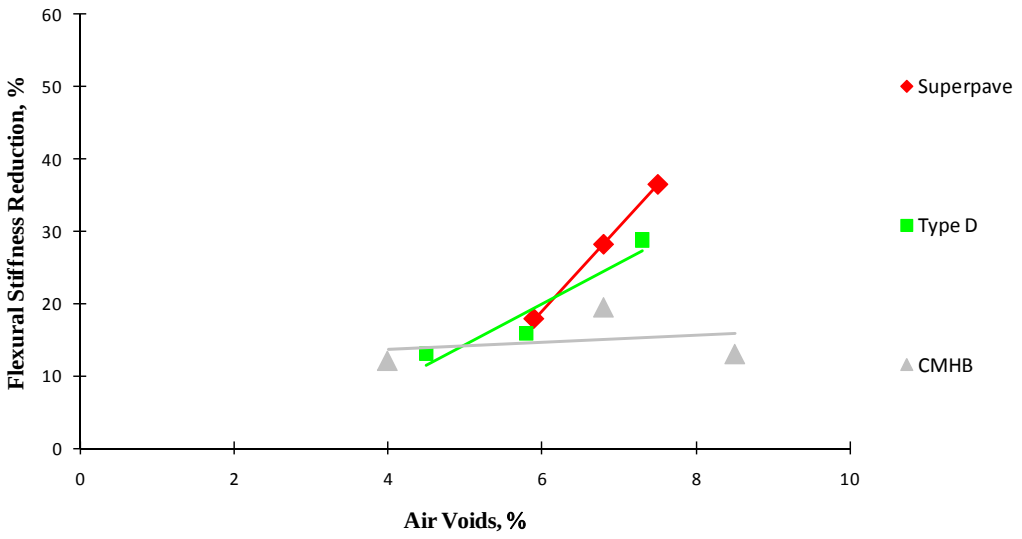

Figure 4.5 – Air Voids Variations Results for All Mixes

Chapter5

Conclusion and Findings

The objective of this thesis was to assess the repeatability of four-point bending method for estimating fatigue cracking of hot mix asphalt. This experimental research has examined the influence of mix proportions, specifically asphalt and air void contents, on fatigue behavior of asphalt beam specimens in the laboratory testing with four-point bending method of loading. The different test conditions regarding to temperatures and loading frequencies were conducted on synthetic specimen and four different asphalt mixes. The study also explored the effect of different environmental changes and mix properties on the behavior of asphalt under the fatigue failure conditions. Specific findings are as below:

1. The obtained results show repeatability on four-point bending method. The results are reasonably repeatable with an average of about 19.6% for flexural stiffness reduction for all testes specimens. This level of variability is supported by the 35.7% COV of air voids.

2. The flexural stiffness reduction is significantly impacted by the temperature for all mixes. For controlled-strain loading configuration, a decrease in temperature results in a decrease in mix stiffness and as consequently an increase in laboratory fatigue life of all specimens. The fatigue failure occurred for all mixes in low temperature of 4.4 ^{o}C.

3. For controlled-strain testing, an increase in air-void content results in a decrease in laboratory fatigue life and a decrease in mix stiffness. For all mixes the initial flexural stiffness is greater for the medium air voids as compared to the low and high air voids.

4. The basic effect of different strains is not as significant as test temperature. The rate of flexural strength reduction is significantly greater between 400 με and 600 με levels than 200 με to 400 με levels. Although the more reduction in flexural stiffness were reported for the higher strain (600 με).

5. The impact of the frequency on the measured parameters in the range of frequencies of 5 to 15 Hz is rather small and within the magnitude of uncertainties anticipated due to variations in the uniformity of the specimens.

6. Another important consideration in this test method is quality control. With respect to fatigue performance, accurate control of air-void content is very important than accurate control of asphalt content.

7. The Superpave and Type mixes compare to PFC and CMHB mixes had the bigger amounts of flexural stiffness for all parametric studies conditions.

References

ASTM, D4123-82, (1995), "Standard Test Method for Indirect Tension Test for Resilient Modulus of Bituminous Mixtures," (Withdrawn, 2003).

Australian Asphalt Association, (2005), "Commentary to AG: PT/T220- Sample Preparation-Compaction of Asphalt Slabs Suitable for Characterization, <http://www.austroads.com.au/pdf/TestMethod/T220_Slab_Compaction.pdf>, (September, 2005).

Bhattacharjee, S., (2005), "Use of Accelerated Loading Equipment for Fatigue Characterization of Hot Mix Asphalt in the Laboratory," Department of Civil and Environmental Engineering, Worcester Polytechnic Institute, (January, 2005).

Brown, S.F., (1996), "Geosynthetics in Asphalt Pavement," International Geosynthetic Society, <http://geosynthetica.net/tech_docs/igs_pavements.pdf >

Brown, E.R., Kandhal, P.S., and Zhang, J., (2001), "Performance Testing for Hot Mix Asphalt," NCAT Report 01-05A, National Center for Asphalt Technology Auburn University, Alabama.

Germann, F.P., and Lytton, R.L., (1979), "Methodology for Predicting the Reflection Cracking Life of Asphalt Concrete Overlays," Research Report, FHWA/TX-79/09+207-5, College Station, Texas.

Harvely, J.T., Deacon, J.A., Tsai, B.W., and Monismith, C.L., (1995), "Fatigue Performance of Asphalt Concrete Mixed and its Relationship with Asphalt Concrete Pavement Performance in California," California Department of Transportation, University of California at Berkeley, RTA-65W485-2, (October, 1995).

Huang, H.Y., (2002), "Pavement Analysis, and Design," Prentice Hall-Englewood, Cliffs, NJ, (2002).

Kaloush, K.E., Witczak, M.W., and Way, G.B., (2002), "Performance Evaluation of Arizona Asphalt Rubber Mixtures Using Advanced Dynamic Material Characterization Tests," College of Engineering, and Applied Sciences, Department of Civil and Environmental Engineering of Arizona State University, (July, 2002).

Lee, S., Seo, Y., and Kim, Y.R., (2006), "Experimental Validation of Laboratory Performance Models Using The Third Scale Accelerated Pavement Testing," KSCE Journal of Engineering, Vol. 10, No.1.

Lefeuvre, Y., de La Roche, C., and Piau, J.M., (2004), "Asphalt Material Fatigue Test under Cyclic Loading: The Lengthening of Samples as a Way to Characterize the Material Damage Experiments and Modeling," Materials, and Structures 38, (January-February 2005) 115-119, (March, 2004).

Liang, R.Y., and Zhou, J., September, (1996), "Prediction of Fatigue Life of Asphalt Concrete Beams," Department of Civil Engineering, Center for Infrastructure Materials and Rehabilitation, University of Akron, (September, 1996).

Li, Y., and Metcalf, J.B., (2004), "Fatigue Characteristics of Asphalt Concrete from Asphalt Slab Tests," Journal of Materials in Civil Engineering, ASCE, (August, 2004).

Mun, S., Guddati, M., and Kim, Y., (2006), "Visco-Elastic Continuum Damage Finite Element Modeling of Asphalt Pavements for Fatigue Cracking Evaluation," KSCE., Journal of Civil Engineering, Vol., 10, No., 2, (March, 2006).

Paris, J., Pereira, P., and Picado-Santos, L., (2002), "Variability of Laboratory Fatigue Life of Asphalt Mixes Using Four Point Bending Test Results," Department of Civil Engineering, University of Minho, Portugal., IPJ, 2002, Volume 1, Number 2, (May , 2002).

Portillo, O., (2008), "Experimental Investigation of the Fracture Mechanics of Bituminous Mixes", BSSM International Conference on Advances in Experimental Mechanics, The National Physical Laboratory (NPL), London, U K, (2008).

Raad, L., Saboundjian, S., and Minassian, G., "Field Aging Effects on the Fatigue of Asphalt Concrete, and Asphalt-Rubber Concrete," University of Alaska, Fairbanks, (2001).

Reyes, J., Mahmoud, E., Abdallah, E., Masad, E., Nazarian, S., and Tandon, V., (2008), "Quantifying the Role of Coarse Aggregate Strength on Resistance to Load in HMA", Center for Transportation Infrastructure Systems The University of Texas at El Paso, Texas Department of Transportation Research Report, FHWA/TX 08/0-5268-2, (June, 2008).

Signore, S.J.M., Wu, R., Santucci, L., and Harvey, J.T., (2006), "Summary and Recommendations Toward Implementing Innovations Based on Selected Presentations at the Asphalt Rubber Pavement Conference," University of California-Pavement Research Center UC Davis and Berkeley, (October, 2006).

Tangella, R., Craus, J., Deacon, J., and Monismith, J., (1990), "Summary Report on Fatigue Response of Asphalt Mixture," Institute of Transportation Studies, University of California Berkeley, California, (February, 1990).

Thom, N., (2006), "Asphalt Cracking: a Nottingham Perspective," University of Nottingham, Nottingham Center for Pavement Engineering, Nottingham, NG7 2RD, UK," (November 26, 2006).

Tigdemir, M., Kalyoncuoglu, S.F., and Kalyoncuoglu, Y.U., "Application of Ultrasonic Method in Asphalt Concrete Testing for Fatigue Life Estimation," University of Sdu Mmf Insaat Muh Bol., Isparta., 32260, Turkey., (March, 2004).

Walubita, F.L., Martin, A.E., Jung, S.H., Glover, C.J., Chowdhurry, A., Park E.S., and Lytton, R.L., "Preliminary Fatigue Analysis of A Common TxDOT Hot Mix Asphalt Concrete Mixture," Texas Transportation Institute and the Texas A&M University System., FHWA/TX-05/0-4468-1, (April, 2004).

White, T.D., Haddock, J.E, Hand, A.J.T., and Fang, H., (2002), "Contributions of Pavement Structural Layers to Rutting of Hot Mix Asphalt Pavements," National Cooperative Highway Research Program NCHRP, Report 468, (2002).

Wolters, R.O., and Holts, D., "Asphalt Pavement Design Guide," Minnesota Asphalt Pavement Association, <http://asphaltisbest.com/>

Zhou, F., and Scullion, T., (2004), "Over Layer Tester: a Rapid Performance Related Crack Resistance Test," Texas Department of Transportation and the Federal Highway Administration, FHWA/TX-05/0-4467-2, (October, 2004).

Zhou F., Hu, S., and Scullion, T., (2007), "Development and Verification of the Overlay Tester Based Fatigue Cracking Prediction Approaches," Texas Transportation Institute the Texas A&M University System College Station, FHWA/TX-07/9-1502-01-8, (January, 2007).

Appendix A

GLOSSARY

Basic definitions for some commonly terms used in asphalt terminology was used in this research are in table (Signore et al., 2006).

American Society for Testing and Materials (ASTM)	Governing body for standards development in the United States
Binder	Asphalt cement. May be modified with polymers or rubber.
Dynamic Modulus (E*)	Dynamic modulus (E*) refers to the bending stiffness under repeated loading of a visco-elastic material which has both magnitude and phase components. With visco-elastic materials, there is a time lag between the applied stress and resulting strain (and vice-versa) in the material. The time lag is represented by the phase component of E*, noted as φ.
Elastic modulus	The stiffness of an asphalt concrete mix as measured by the ratio of applied stress to resulting strain within the material.

Appendix B

FATIGUE TESTS RESULTS FOR ALL MIXES

Table B.1 – Repeatability Results for Superpave Specimens

Specimen	Air Voids Content, %	Flexural Stiffness, MPa		Flexural Stiffness Reduction,%	Modulus of Elasticity, MPa (from IPC)		Ultra Sonic Results: V-meter	
		Initial	Final		Initial	Final	Modulus of Elasticity, MPa	COV, %
1	7.2	1259	889	29.4	1362	961	4907	3.3
2	6.8	1343	1013	24.6	1439	1085	4527	5.8
3	6.5	1330	977	26.5	1430	1051	4310	2.5
Average	6.8	1311	960	26.8	1410	1032	4581	3.8
COV, %	5.1	3.5	6.6	9.0	3.0	6.2	6.6	-

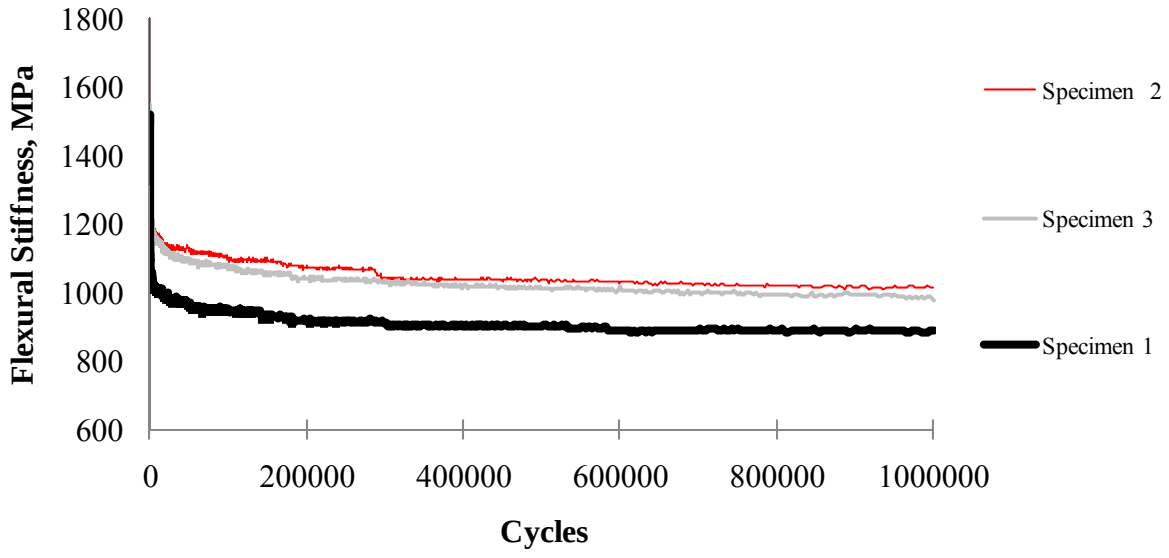

Figure B.1 – Repeatability Results for Superpave Specimens

Table B.2 – Repeatability Results for Type D Specimens

Specimen	Air Voids Content, %	Flexural Stiffness, MPa		Flexural Stiffness Reduction,%	Modulus of Elasticity, MPa (from IPC)		Ultra Sonic Results: V-meter	
		Initial	Final		Initial	Final	Modulus of Elasticity, MPa	COV, %
1	7.3	1234	879	28.8	1328	1018	4504	3.6
2	7.2	1077	816	24.3	1167	884	4820	5.2
3	4.6	1096	880	19.7	1172	941	3478	7.4
Average	6.4	1136	858	24.2	1222	948	4267	5.4
COV, %	24.2	7.5	4.3	18.7	7.5	7.1	16.4	-

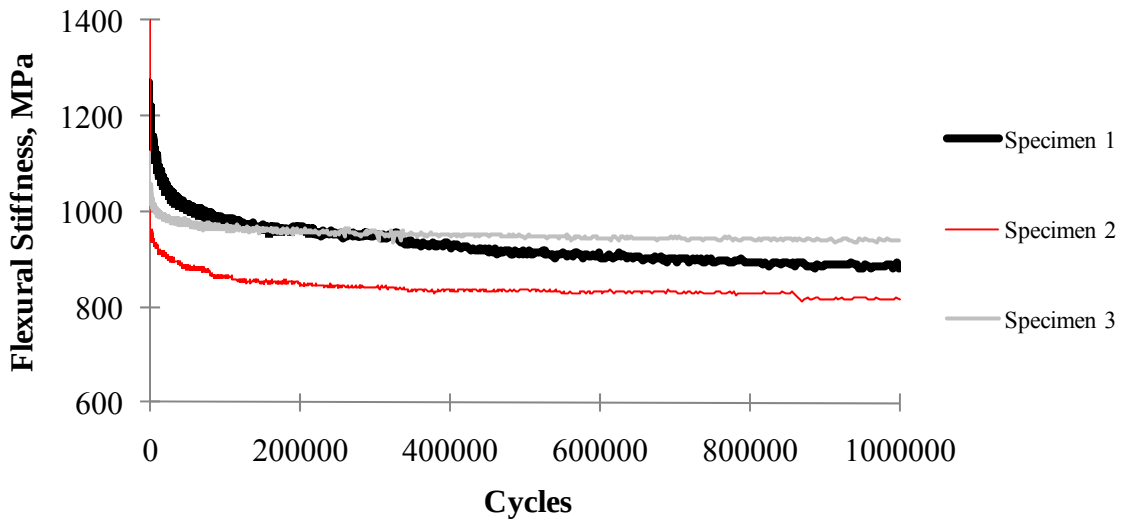

Figure B.2 – Repeatability Results for Type D Specimens

Table B.3 – Repeatability Results for CMHB Specimens

Specimen	Air Voids Content, %	Flexural Stiffness, MPa		Flexural Stiffness Reduction,%	Modulus of Elasticity, MPa (from IPC)		Ultra Sonic Results: V-meter	
		Initial	Final		Initial	Final	Modulus of Elasticity, MPa	COV, %
1	5.0	1168	1005	14.0	1246	1071	3937	8.8
2	6.8	1280	1030	19.5	1365	1099	3526	6.5
3	5.9	1219	1078	11.6	1297	1147	3694	7.0
Average	5.9	1223	1037	15.1	1303	1105	3719	7.5
COV, %	15.2	4.6	3.6	27.0	4.6	3.4	5.6	-

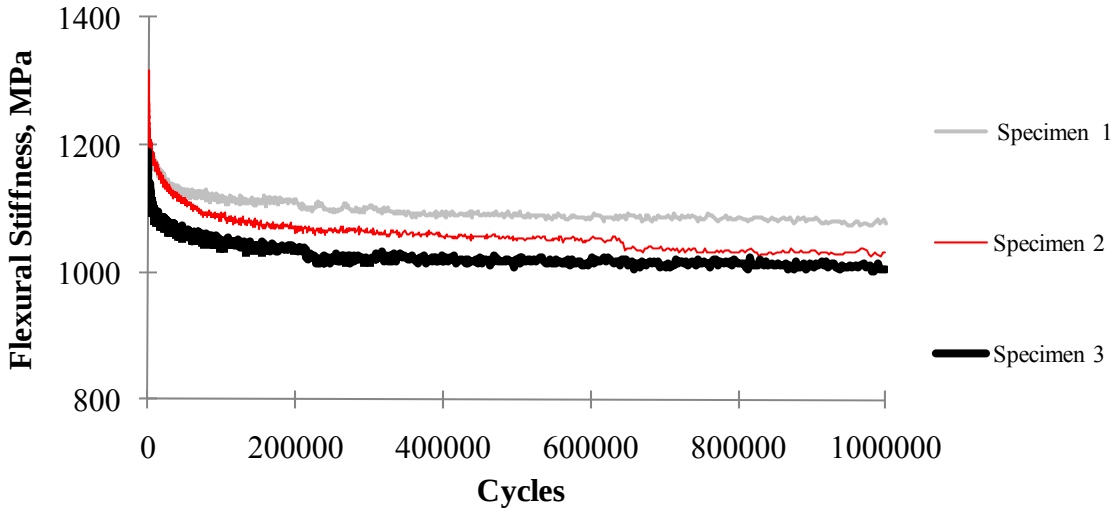

Figure B.3 – Repeatability Results for CMHB Specimens

Table B.4 – Repeatability Results for PFC Specimens

Specimen	Air Voids Content, %	Flexural Stiffness, MPa		Flexural Stiffness Reduction,%	Modulus of Elasticity, MPa (from IPC)		Ultra Sonic Results: V-meter	
		Initial	Final		Initial	Final	Modulus of Elasticity, MPa	COV, %
1	15.3	1098	1054	4.0	1165	1118	1965	8.8
2	15.2	1162	914	21.3	1235	972	1851	3.7
3	16.2	1021	905	11.4	1093	968	1647	6.2
Average	15.6	1094	957	12.3	1165	1019	1821	6.3
COV, %	3.6	6.4	8.7	70.7	6.1	8.4	8.9	-

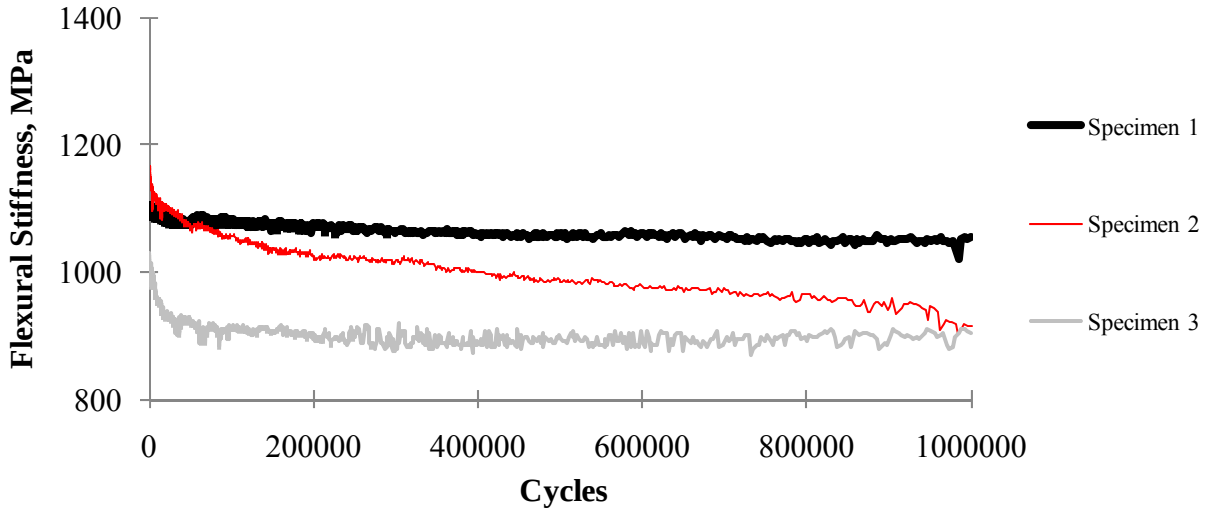

Figure B.4 – Repeatability Results for PFC Specimens

Table B.5 – Frequency Results for Superpave Specimens

Specimen	Frequency, Hz	Air Voids Content, %	Flexural Stiffness, MPa		Flexural Stiffness Reduction,%	Modulus of Elasticity, MPa		Ultra Sonic Results: V-meter	
			Initial	Final		Initial	Final	Modulus of Elasticity, MPa	COV, %
1	5	6.6	1508	1043	30.8	1621	1121	4749	6.0
2	10	6.8	1410	1013	28.2	1511	1085	4527	5.8
3	15	6.4	1398	882	36.9	1497	944	4317	3.4

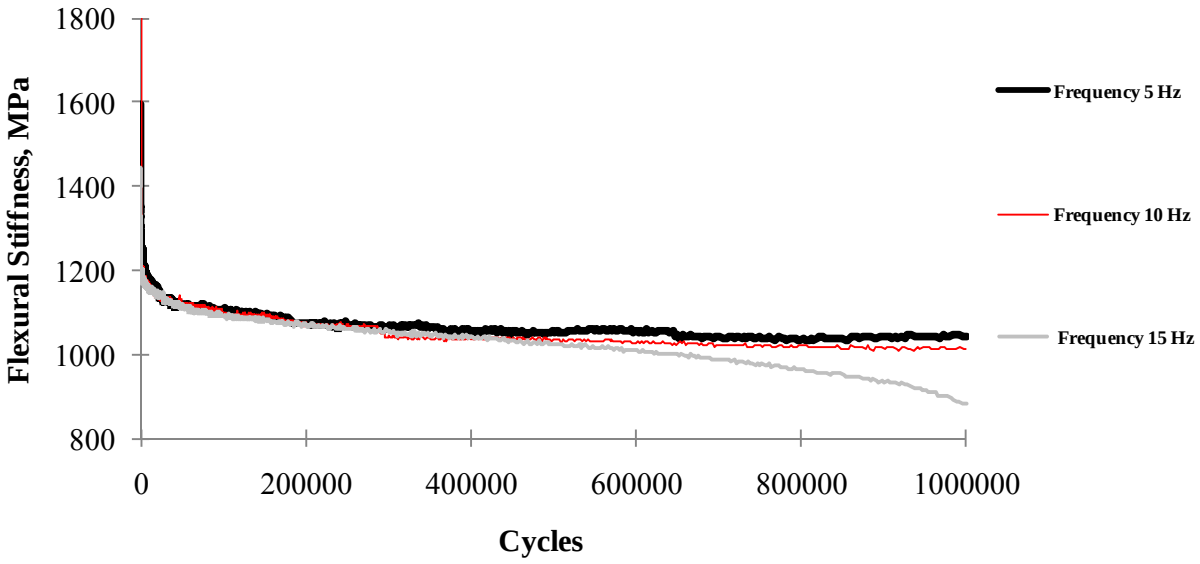

Figure B.5 – Frequency Results for Superpave Specimens

Table B.6 – Frequency Results for Type D Specimens

Specimen	Frequency, Hz	Air Voids Content, %	Flexural Stiffness, MPa		Flexural Stiffness Reduction,%	Modulus of Elasticity, MPa		Ultra Sonic Results: V-meter	
			Initial	Final		Initial	Final	Modulus of Elasticity, MPa	COV, %
1	5	5.8	1238	896	27.7	1334	965	4002	4.1
2	10	7.3	1234	879	28.8	1328	1018	4504	3.6
3	15	6.9	1446	981	32.2	1556	1056	4610	6.1

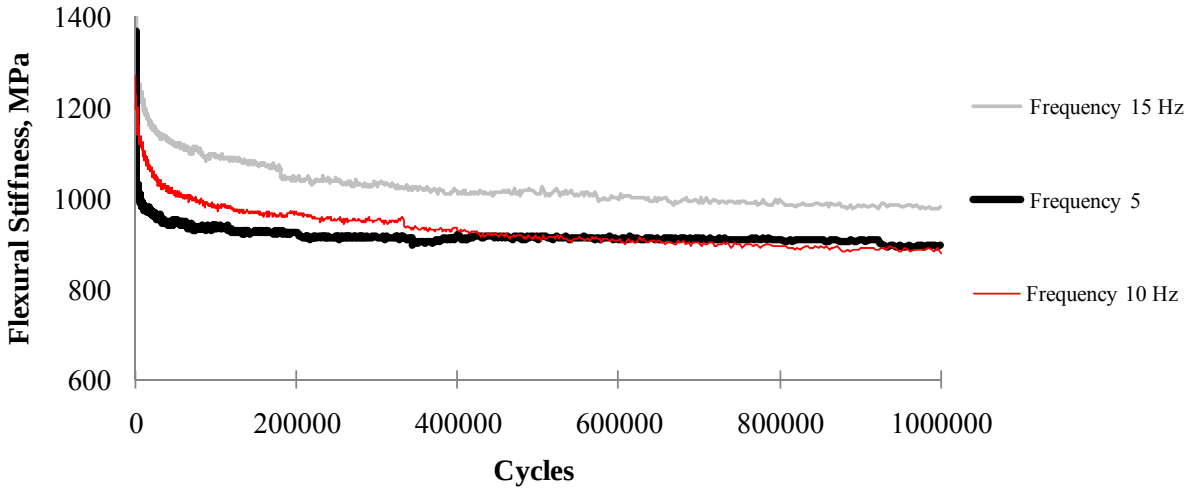

Figure B.6 – Frequency Results for Type D Specimens

Table B.7 – Frequency Results for CMHB Specimens

Specimen	Frequency, Hz	Air Voids Content, %	Flexural Stiffness, MPa		Flexural Stiffness Reduction,%	Modulus of Elasticity, MPa		Ultra Sonic Results: V-meter	
			Initial	Final		Initial	Final	Modulus of Elasticity, MPa	COV, %
1	5	7.0	1111	1005	9.5	1182	1070	3557	7.9
2	10	5.9	1219	1078	11.6	1297	1147	3694	7.0
3	15	5.9	1076	913	15.1	1150	976	3571	6.8

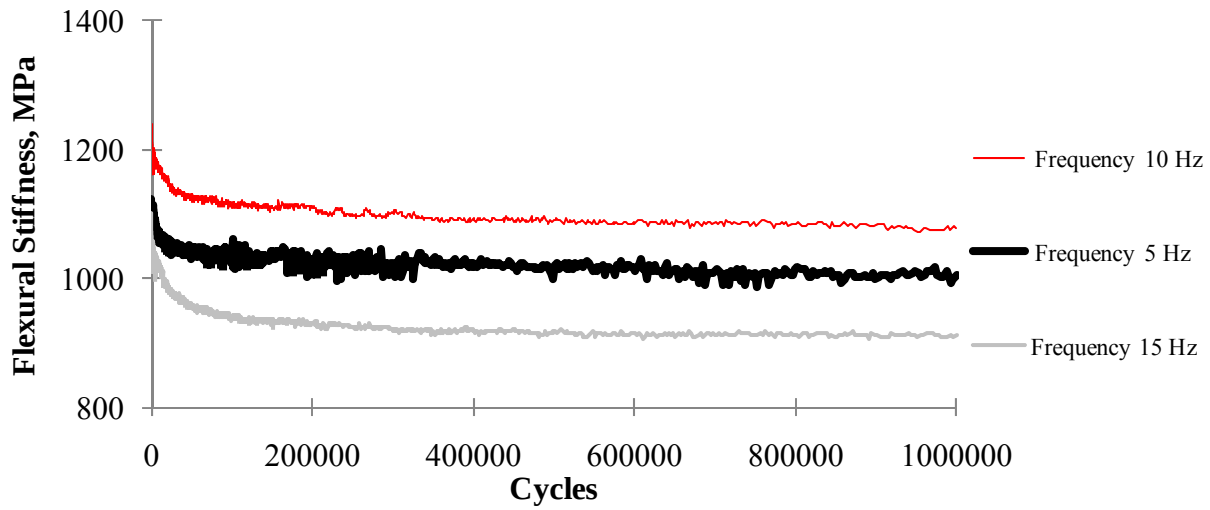

Figure B.7 – Frequency Results for CMHB Specimens

Table B.8 – Frequency Results for PFC Specimens

Specimen	Frequency, Hz	Air Voids Content, %	Flexural Stiffness, MPa		Flexural Stiffness Reduction,%	Modulus of Elasticity, MPa		Ultra Sonic Results: V-meter	
			Initial	Final		Initial	Final	Modulus of Elasticity, MPa	COV, %
1	5	17.8	1113	1015	8.8	1180	1076	1782	11.2
2	10	16.2	1021	905	11.4	1093	968	1647	6.2
3	15	13.5	1166	1049	10.0	1240	1116	1904	5.7

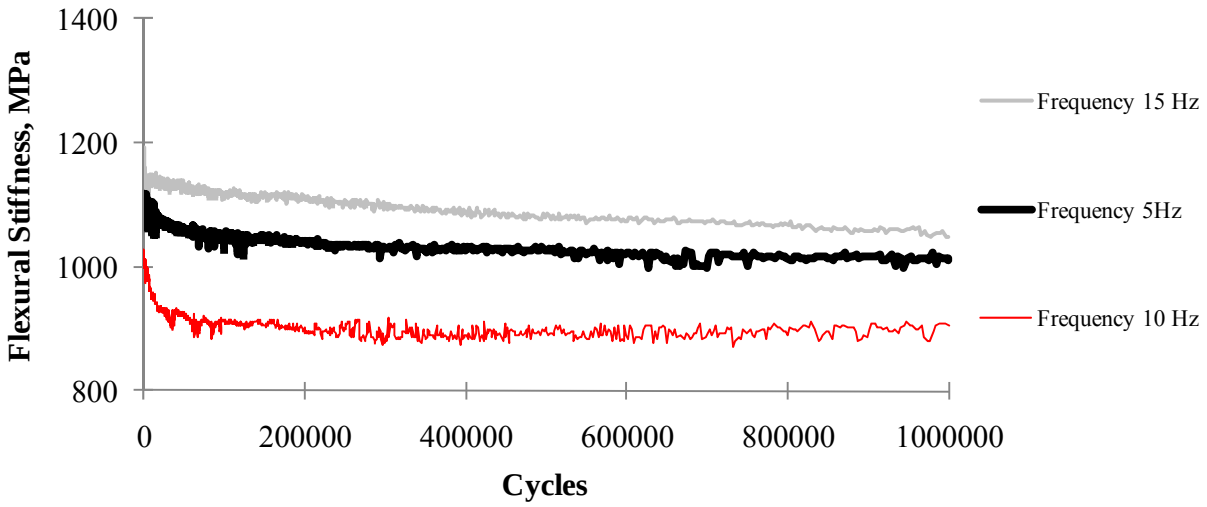

Figure B.8 – Frequency Results for PFC Specimens

Table B.9 – Strain Variations Results for Superpave Specimens

Specimen	Strain, με	Air Voids Content, %	Flexural Stiffness, MPa		Flexural Stiffness Reduction,%	Modulus of Elasticity, MPa		Ultra Sonic Results: V-meter	
			Initial	Final		Initial	Final	Modulus of Elasticity, MPa	COV, %
1	200	6.1	1695	1321	22.1	1822	1420	4843	2.3
2	400	6.8	1410	1013	28.2	1511	1085	4527	5.8
3	600	6.0	1124	557	50.4	1202	596	4967	2.2

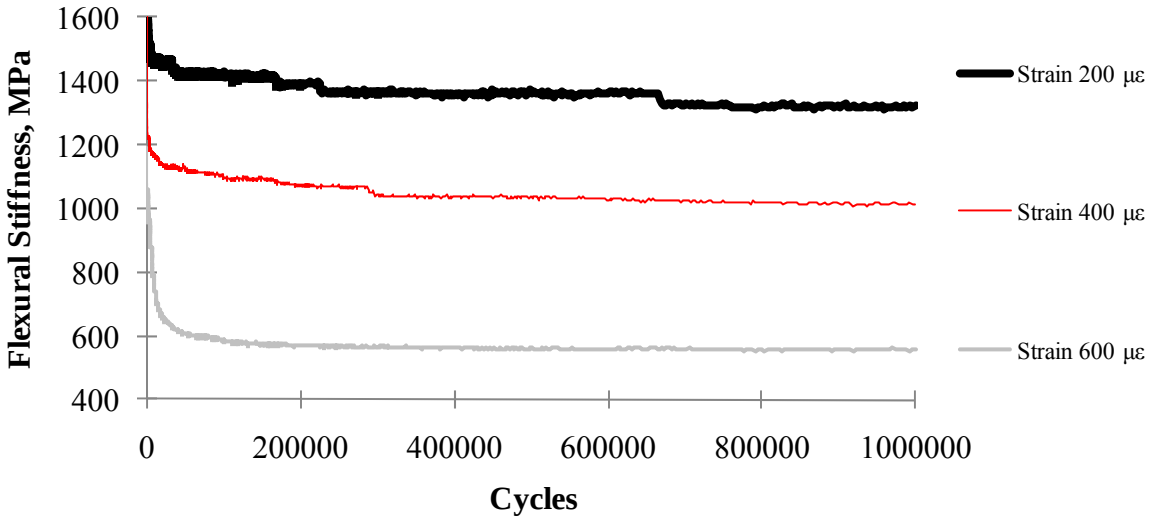

Figure B.9 – Strain Variations Results for Superpave Specimens

Table B.10 – Strain Variations Results for Type D Specimens

Specimen	Strain, με	Air Voids Content, %	Flexural Stiffness, MPa		Flexural Stiffness Reduction,%	Modulus of Elasticity, MPa		Ultra Sonic Results: V-meter	
			Initial	Final		Initial	Final	Modulus of Elasticity, MPa	COV, %
1	200	7.4	1340	1196	10.8	1427	1273	4858	2.6
2	400	7.2	1054	896	15.0	1131	961	4820	5.2
3	600	6.5	984	669	32.1	1063	722	4070	6.7

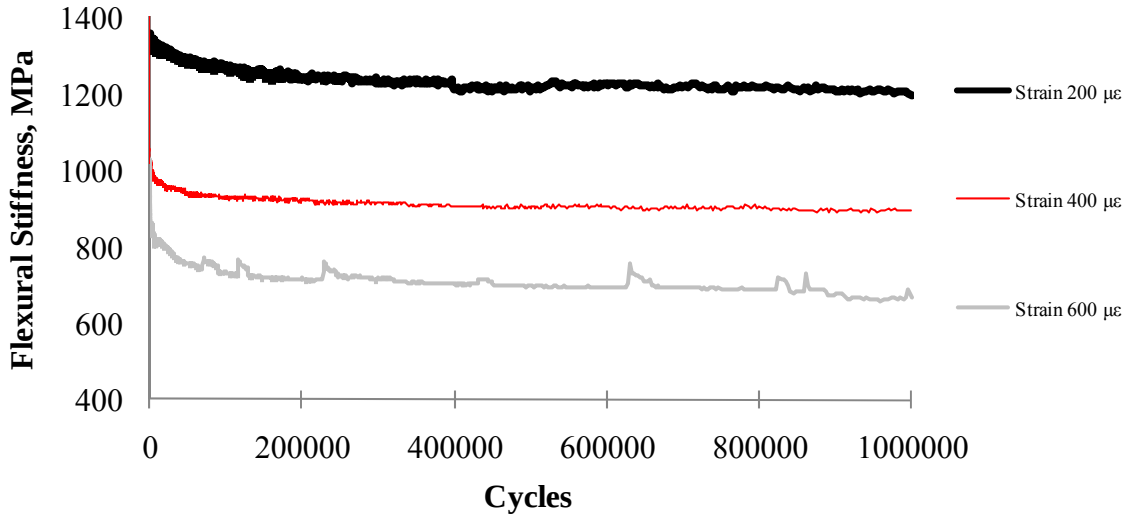

Figure B.10 – Strain Variations Results for Type D Specimens

Table B.11 – Strain Variations Results for CMHB Specimens

Specimen	Strain, με	Air Voids Content, %	Flexural Stiffness, MPa		Flexural Stiffness Reduction,%	Modulus of Elasticity, MPa		Ultra Sonic Results: V-meter	
			Initial	Final		Initial	Final	Modulus of Elasticity, MPa	COV, %
1	200	5.8	1107	1034	6.6	1183	1105	3644	6.6
2	400	5.9	1219	1078	11.6	1297	1147	3694	7.0
3	600	6.0	1279	1064	16.8	1357	1129	3690	4.7

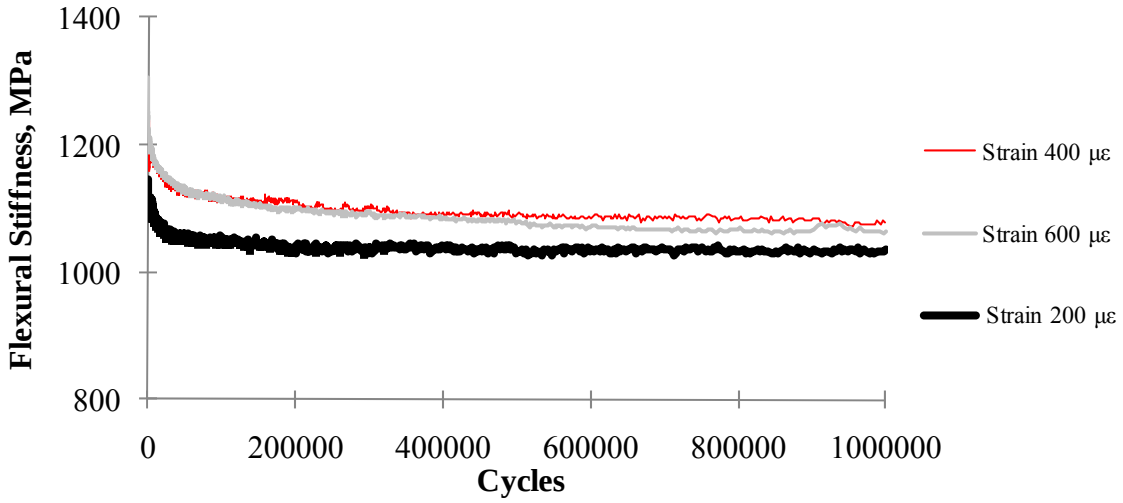

Figure B.11 – Strain Variations Results for CMHB Specimens

Table B.12 – Strain Variations Results for PFC Specimens

Specimen	Strain, με	Air Voids Content, %	Flexural Stiffness, MPa		Flexural Stiffness Reduction,%	Modulus of Elasticity, MPa		Ultra Sonic Results: V-meter	
			Initial	Final		Initial	Final	Modulus of Elasticity, MPa	COV, %
1	200	16.1	1060	1052	0.8	1124	1116	2205	8.2
2	400	17.5	1021	905	11.4	1093	968	1647	6.2
3	600	18.2	967	872	9.8	1032	930	1821	1.7

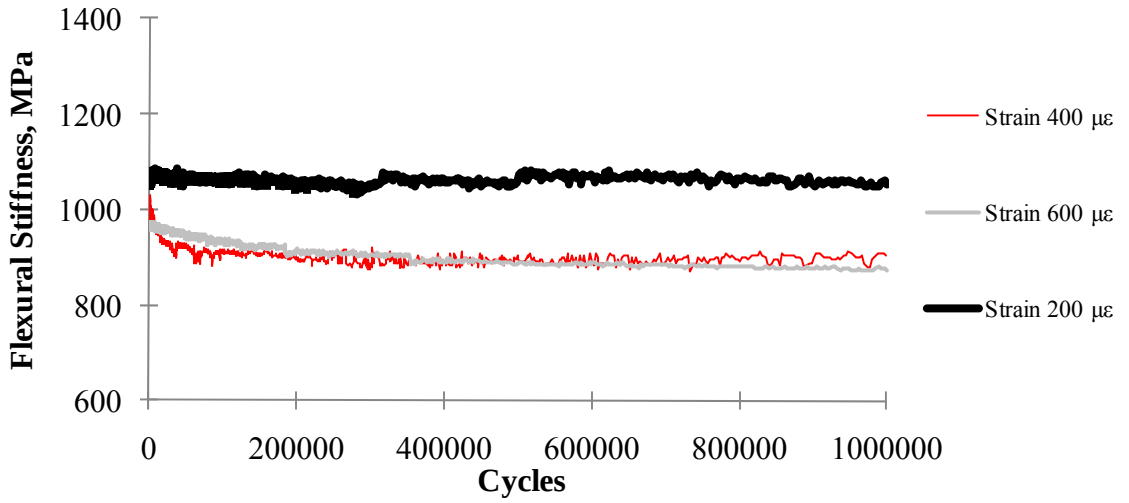

Figure B.12 – Strain Variations Results for PFC Specimens

Table B.13 – Temperature Variations Results for Superpave Specimens

Specimen	Temperature, °C	Air Voids Content, %	Flexural Stiffness, MPa		Flexural Stiffness Reduction,%	Modulus of Elasticity, MPa		Ultra Sonic Results: V-meter	
			Initial	Final		Initial	Final	Modulus of Elasticity, MPa	COV, %
1	4.4	7.0	2411	1385	42.5	2579	1482	4641	9.1
2	21.5	6.8	1410	1013	28.2	1511	1085	4527	5.8
3	37.5	5.7	926	8366	9.7	985	890	4373	5.2

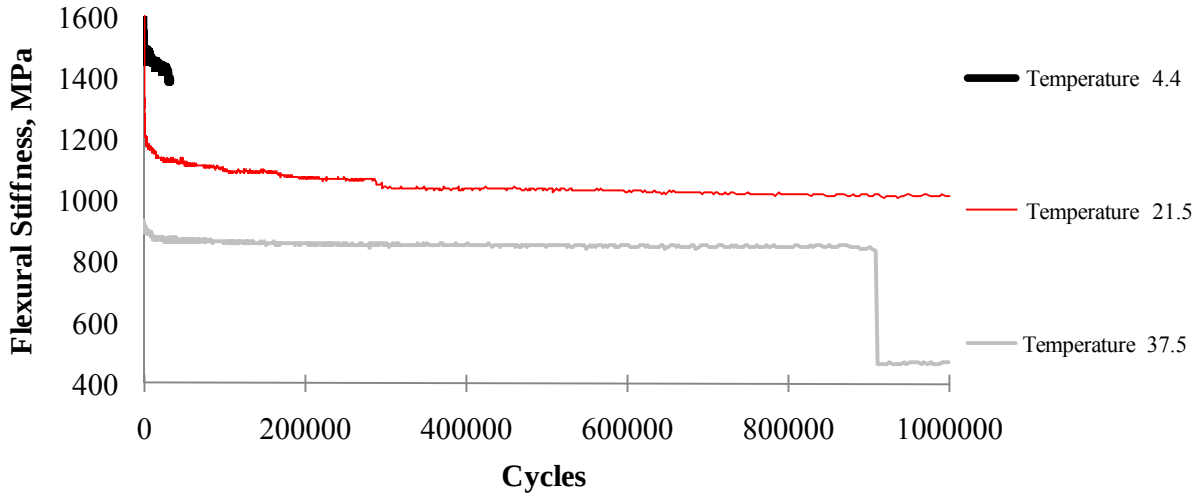

Figure B.13 – Temperature Variations Results for Superpave Specimens

Table B.14 – Temperature Variations Results for Type D Specimens

Specimen	Temperature, °C	Air Voids Content, %	Flexural Stiffness, MPa		Flexural Stiffness Reduction,%	Modulus of Elasticity, MPa		Ultra Sonic Results: V-meter	
			Initial	Final		Initial	Final	Modulus of Elasticity, MPa	COV, %
1	4.4	7.7	1492	712	52.2	1613	770	4287	3.9
2	21.5	6.9	1054	896	15.0	1131	961	4942	5.2
3	37.5	5.2	880	820	6.9	940	875	4330	2.6

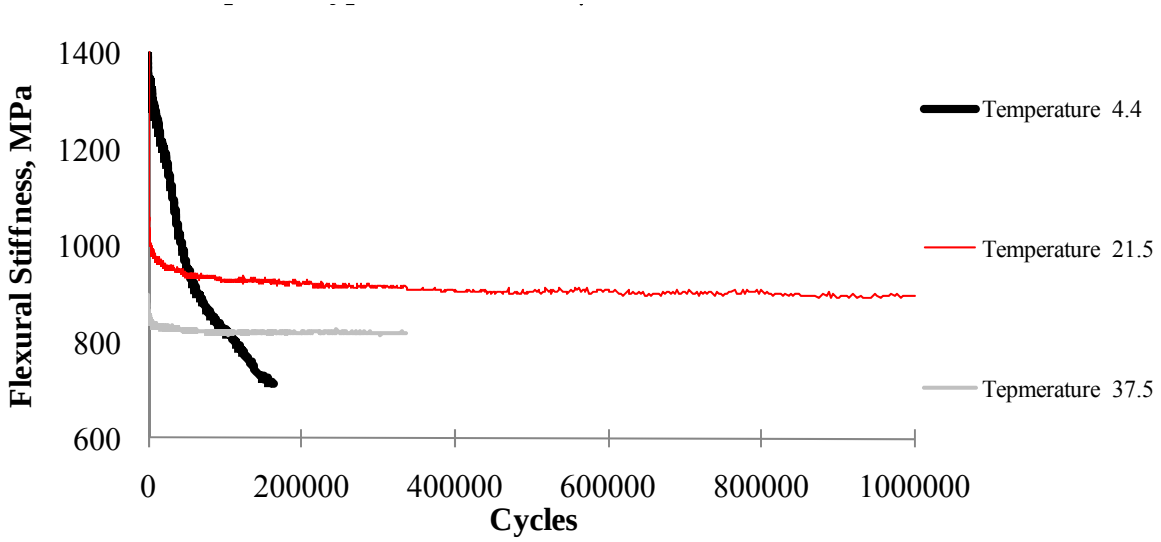

Figure B.14 – Temperature Variations Results for Type D Specimens

Table B.15 – Temperature Variations Results for CMHB Specimens

Specimen	Temperature, °C	Air Voids Content, %	Flexural Stiffness, MPa		Flexural Stiffness Reduction,%	Modulus of Elasticity, MPa		Ultra Sonic Results: V-meter	
			Initial	Final		Initial	Final	Modulus of Elasticity, MPa	COV, %
1	4.4	6.2	1600	803	49.8	1702	854	4220	2.8
2	21.5	5.0	1168	1005	14.0	1246	1071	3937	8.8
3	37.5	5.6	910	853	6.2	969	909	3656	5.4

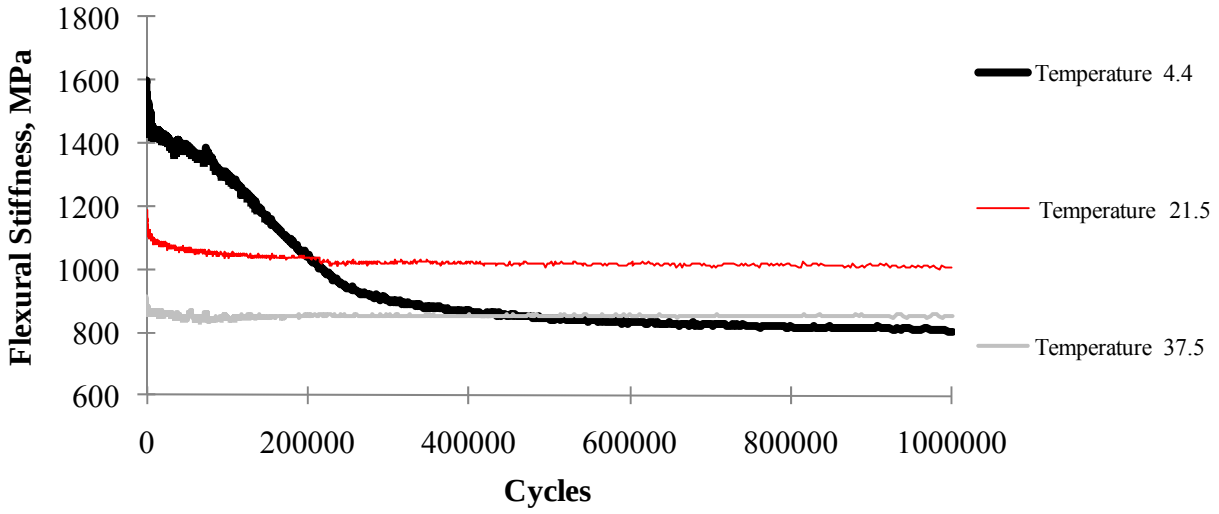

Figure B.15 – Temperature Variations Results for CMHB Specimens

Table B.16 – Temperature Variations Results for PFC Specimens

Specimen	Temperature, °C	Air Voids Content, %	Flexural Stiffness, MPa		Flexural Stiffness Reduction,%	Modulus of Elasticity, MPa		Ultra Sonic Results: V-meter	
			Initial	Final		Initial	Final	Modulus of Elasticity, MPa	COV, %
1	4.4	15.7	1166	1011	13.3	1250	1084	2606	4.1
2	21.5	16.2	1021	905	11.4	1093	968	1647	6.2
3	37.5	16.2	922	896	2.8	982	954	2237	11.2

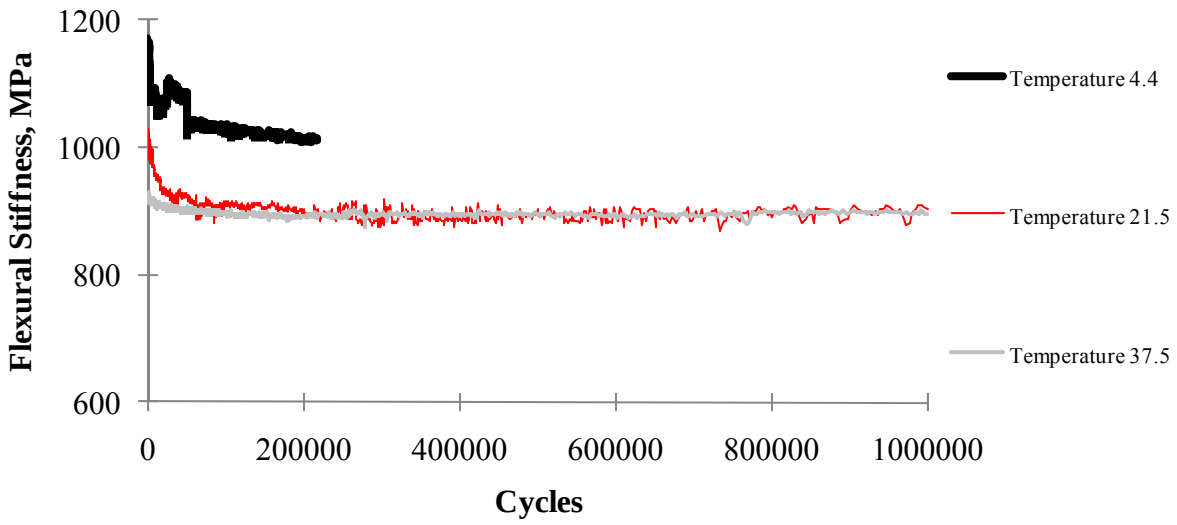

Figure B.16 – Temperature Variations Results for PFC Specimens

Table B.17 – Air Voids Variations Results for Superpave Specimens

Specimen	Air Voids, %	Air Voids Content, %	Flexural Stiffness, MPa		Flexural Stiffness Reduction,%	Modulus of Elasticity, MPa		Ultra Sonic Results: V-meter	
			Initial	Final		Initial	Final	Modulus of Elasticity, MPa	COV, %
1	4	5.9	1171	961	17.9	1248	1032	5199	8.8
2	7	6.8	1410	1013	28.2	1511	1085	6547	5.8
3	11	7.5	1169	742	36.5	1245	791	5902	3.6

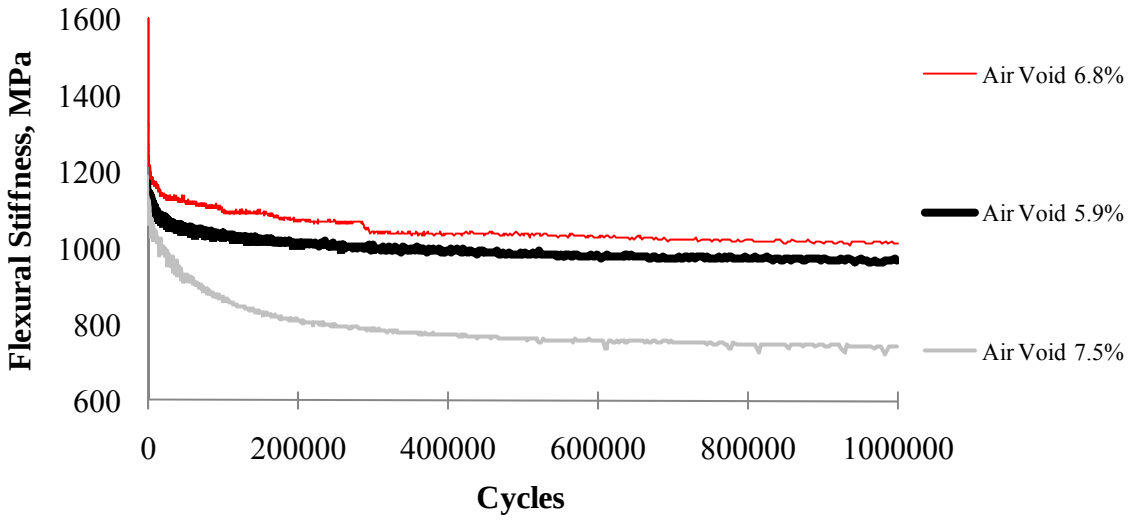

Figure B.17 – Air Voids Variations Results for Superpave Specimens

Table B.18 – Air Voids Variations Results for Type D Specimens

Specimen	Air Voids, %	Air Voids Content, %	Flexural Stiffness, MPa		Flexural Stiffness Reduction,%	Modulus of Elasticity, MPa		Ultra Sonic Results: V-meter	
			Initial	Final		Initial	Final	Modulus of Elasticity, MPa	COV, %
1	4	4.5	1278	1110	13.1	1358	1180	4759	4.4
2	7	5.8	1208	1017	15.8	1288	1085	4504	3.6
3	11	7.3	1234	879	28.8	1328	1018	3615	6.0

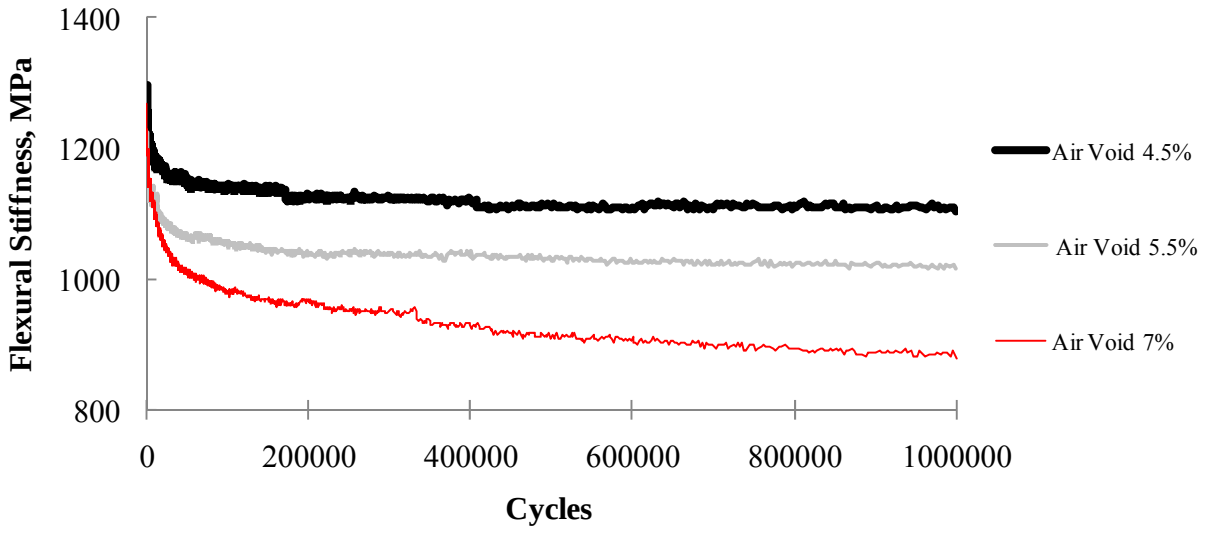

Figure B.18 – Air Voids Variations Results for Type D Specimens

Table B.19 – Air Voids Variations Results for CMHB Specimens

Specimen	Air Voids, %	Air Voids Content, %	Flexural Stiffness, MPa		Flexural Stiffness Reduction,%	Modulus of Elasticity, MPa		Ultra Sonic Results: V-meter	
			Initial	Final		Initial	Final	Modulus of Elasticity, MPa	COV, %
1	4	4.0	1138	1001	12.0	1213	1067	2730	9.1
2	7	6.8	1280	1030	19.5	1365	1099	3526	6.5
3	11	8.5	1153	1003	13.0	1229	1070	3877	7.0

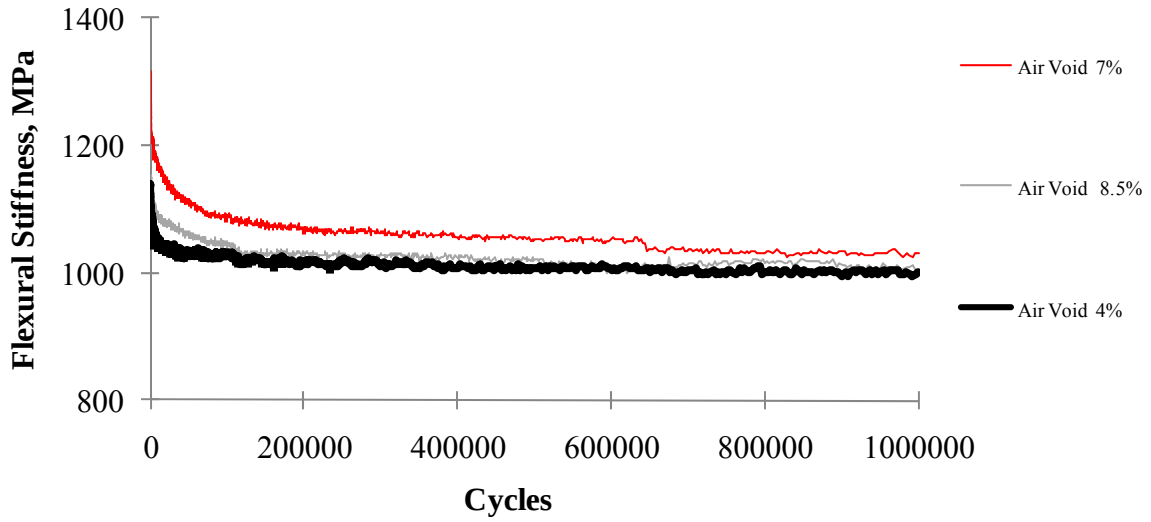

Figure B.19 – Air Voids Variations Results for CMHB Specimens

Appendix C

FATIGUE TESTS RESULTS FOR SYNTHETIC SPECIMEN TRIALS

Table C.1 – Frequency Variations Results for Synthetic Specimens

a- Flexural Stiffness

Trial No.	Flexural Stiffness, MPa								
	10 Hz			15 Hz			20 Hz		
	Initial	Final	Reduction, %	Initial	Final	Reduction, %	Initial	Final	Reduction, %
1	1069	1067	0	1080	1080	0	1086	1083	0
2	1062	1069	0	1087	1083	0	1084	1086	0
3	1072	1069	0	1080	1084	0	1090	1084	1
4	1077	1072	0	1064	1067	0	1069	1072	0
5	1071	1073	0	1065	1069	0	1075	1073	0
Average	1070	1070	0	1075	1077	0	1079	1079	0
COV,%	0.5	0.2	-	0.9	0.7	-	0.9	0.7	-

b- Modulus of Elasticity

Trial No.	Modulus of Elasticity, MPa					
	10 Hz		15 Hz		20 Hz	
	Initial	Final	Initial	Final	Initial	Final
1	1139	1137	1158	1148	1173	1157
2	1132	1139	1155	1155	1151	1155
3	1142	1139	1155	1152	1156	1154
4	1148	1142	1138	1135	1146	1138
5	1141	1143	1130	1139	1142	1142
Average	1140	1140	1147	1146	1149	1147
COV, %	0.5	0.2	1.1	0.7	0.5	0.8

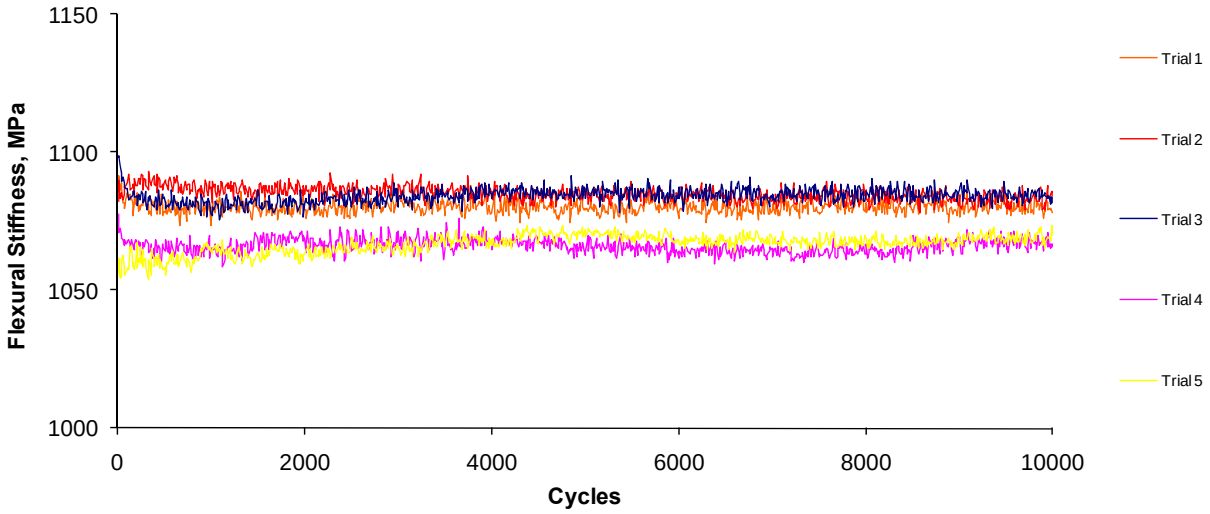

Figure C.1 – Frequency Variations Results for Synthetic Specimens for 15 Hz

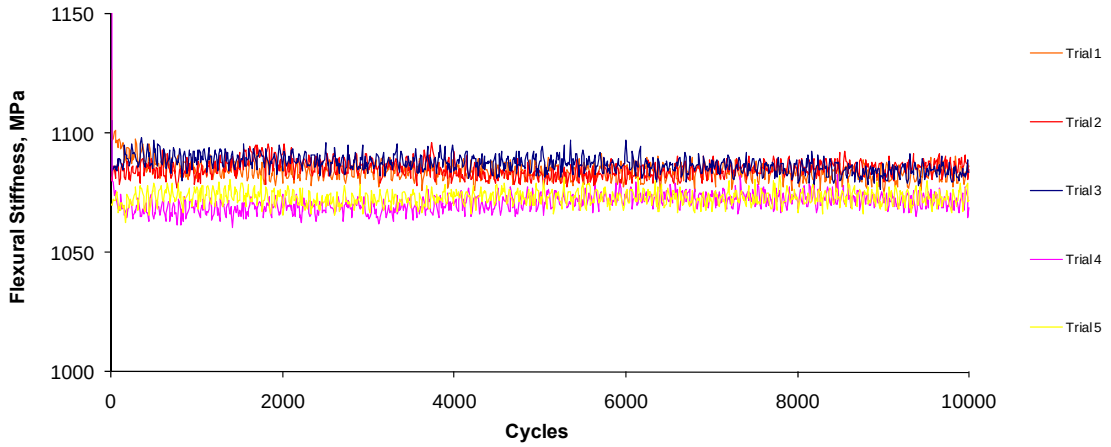

Figure C.2 – Frequency Variations Results for Synthetic Specimens for 20 Hz

Table C.2 – Strain Variations Results for Synthetic Specimens

a- Flexural Stiffness

Trial No.	Flexural Stiffness, MPa								
	200 με			400 με			600 με		
	Initial	Final	Reduction, %	Initial	Final	Reduction, %	Initial	Final	Reduction, %
1	1074	1068	1	1069	1067	0	1084	1082	0
2	1056	1060	0	1062	1069	0	1076	1081	0
3	1059	1049	1	1072	1069	0	1084	1070	1
4	1054	1049	0	1077	1072	0	1081	1076	1
5	1044	1036	1	1071	1073	0	1068	1066	0
Average	1057	1052	0	1070	1070	0	1079	1075	0
COV,	1.0	1.1	_	0.5	0.2	-	0.6	0.6	_

b- Modulus of Elasticity

Trial No.	Modulus of Elasticity, MPa					
	200 με		400 με		600 με	
	Initial	Final	Initial	Final	Initial	Final
1	1151	1134	1139	1137	1152	1153
2	1143	1127	1132	1139	1144	1149
3	1147	1115	1142	1139	1154	1134
4	1116	1120	1148	1142	1149	1143
5	1118	1104	1141	1143	1133	1133
Average	1135	1120	1140	1140	1147	1143
COV, %	1.5	1.0	0.5	0.2	0.7	0.7

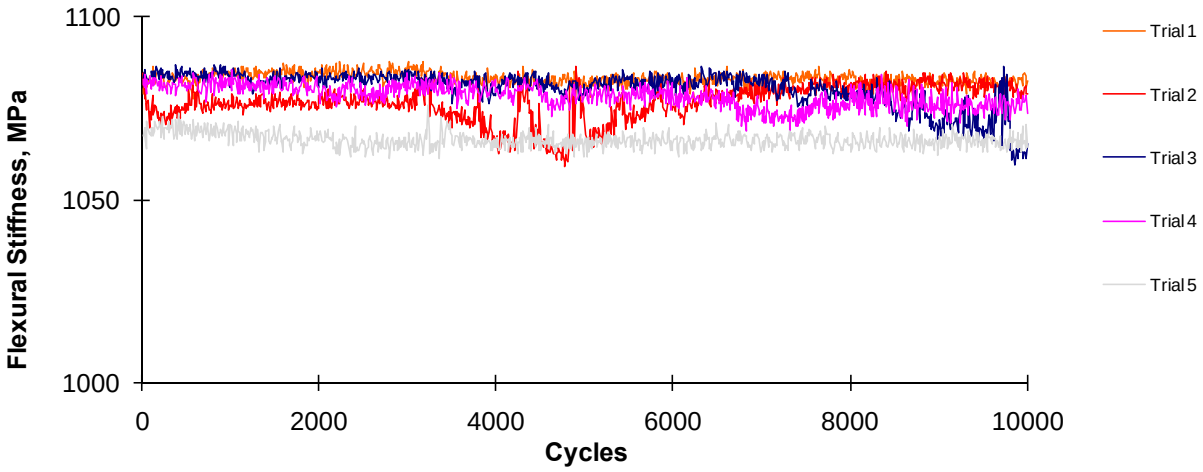

Figure C.3 – Strain Variations Results for Synthetic Specimen for 600 με

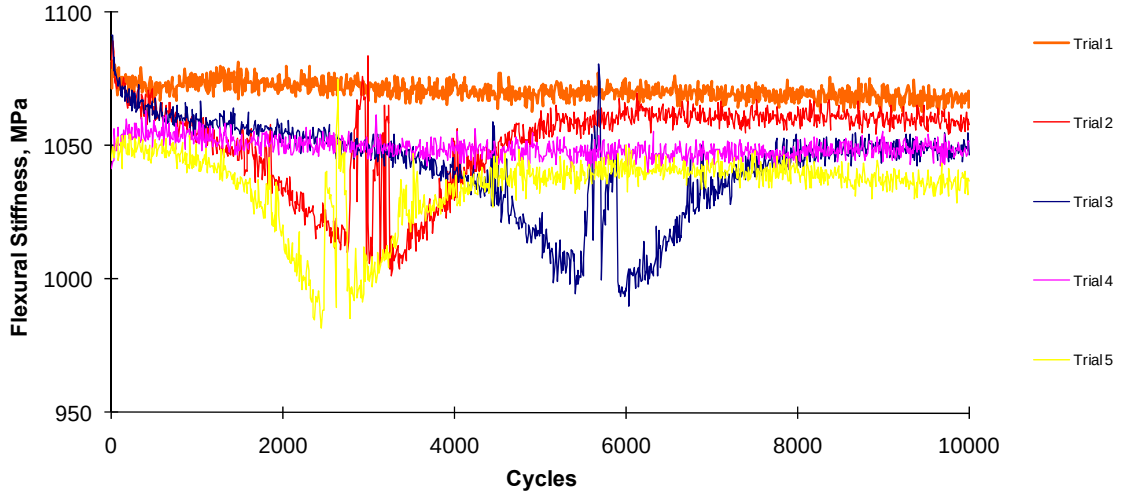

Figure C.4 – Strain Variations Results for Synthetic Specimen for 200 με

Table C.3 – Temperature Variations Results for Synthetic Specimens

a- Flexural Stiffness

Trial No.	Flexural Stiffness, MPa								
	4.4 °C			21.5 °C			37.5 °C		
	Initial	Final	Reduction, %	Initial	Final	Reduction, %	Initial	Final	Reduction, %
1	1073	1075	-0.2	1069	1067	0	1027	1025	0.2
2	1086	1062	2.2	1062	1069	0	1028	1025	0.3
3	1095	1060	3.1	1072	1069	0	1028	1025	0.3
4	1102	1080	2.0	1077	1072	0	1027	1026	0.2
5	1107	1054	4.8	1072	1073	0	1025	1025	0.0
Average	1093	1066	2.4	1070	1070	0	1027	1025	0
COV,%	1.3	1.0	75.3	0.5	0.2	-	0.1	0.0	62.5

b- Modulus of Elasticity

Trial No.	Modulus of Elasticity, MPa					
	4.4 °C		21.5 °C		37.5 °C	
	Initial	Final	Initial	Final	Initial	Final
1	1152	1145	1139	1137	1096	1093
2	1166	1133	1132	1139	1096	1090
3	1180	1133	1142	1139	1091	1092
4	1174	1145	1148	1142	1097	1093
5	1194	1124	1141	1143	1094	1089
Average	1173	1136	1140	1140	1095	1092
COV, %	1.3	0.8	0.5	0.2	0.2	0.2

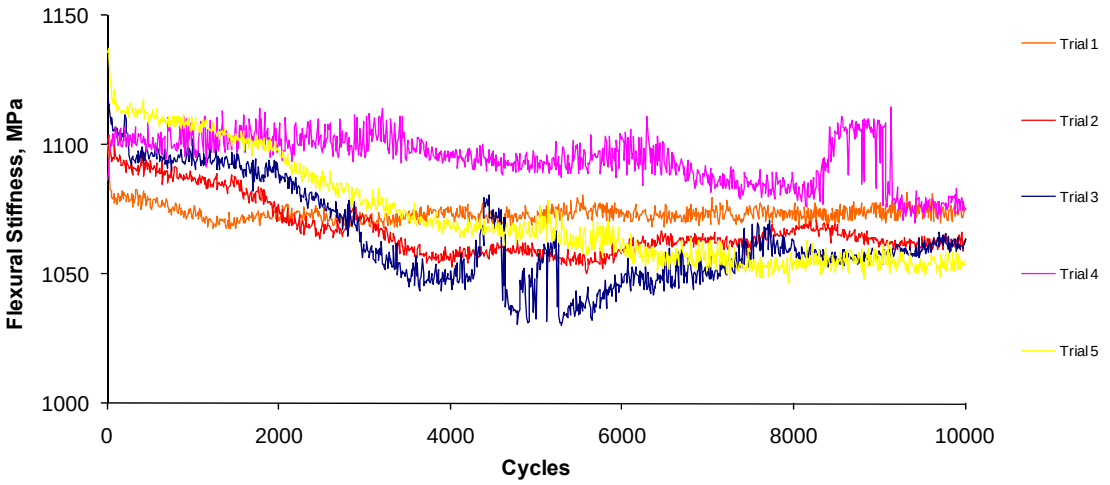

Figure C.5 – Temperature Variations Results for Synthetic Specimen at 4.4 ^{o}C

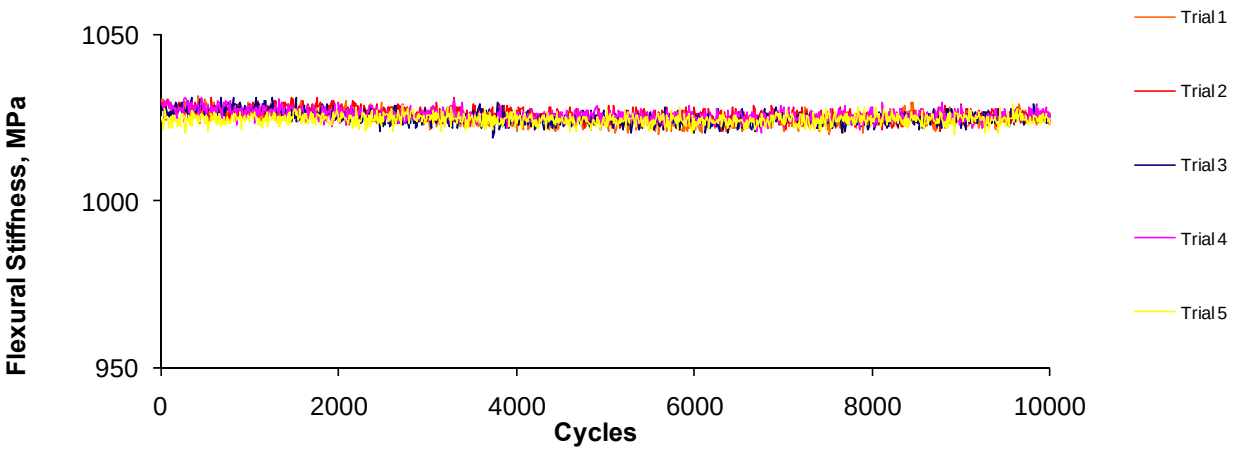

Figure C.6 – Temperature Variations Results for Synthetic Specimen at 37.5 ^{o}C

Curriculum Vita

Sara Montazeri was born on August 27, 1979 in Tehran, Iran. The first daughter of Ali Akbar Montazeri and Simin Heidari, she graduated from Roshd High School in Tehran, Iran in the spring of 1997. In the fall of 2005, she graduated from Iran University of Science and Technology, Tehran, with a Bachelor of Science in Civil Engineering. In the fall of 2007, she entered the graduate school at the University of Texas at El Paso. While pursuing master degrees in civil engineering, she worked as a Graduate Research Assistant at the Center for Transportation Infrastructure Systems (CTIS). She was a recipient of the Eisenhower Fellowship for the academic year, (2008). She was also inducted into the American Society of Civil Engineering (ASCE) in the spring of 2008.

Permanent address: 210 W Redd Road. Apt#616.
El Paso, TX, 79932

This thesis was typed by Sara Montazeri.